2D (< 10 nm) sp3-C-rich carbon materials, possibly hydrogenated: A review

Fabrice Piazza, Marc Monthioux, Pascal Puech

Carbon Trends 9 (2022) 100219

Contents lists available at ScienceDirect

Carbon Trends

journal homepage: www.elsevier.com/locate/cartre

2D (< 10 nm) sp^3-C-rich carbon materials, possibly hydrogenated: A review

Fabrice Piazza[a,*], Marc Monthioux[b], Pascal Puech[b]

[a] Laboratorio de Nanociencia, Pontificia Universidad Católica Madre y Maestra, Autopista Duarte km 1 1/2, Apartado Postal 822, Santiago, Dominican Republic
[b] Centre d'Elaboration des Matériaux et d'Etudes Structurales (CEMES), CNRS, Université de Toulouse, France

ARTICLE INFO

Article history:
Received 29 July 2022
Revised 22 September 2022
Accepted 22 September 2022

Keywords:
Amorphous carbon
Graphane
Diamane
Diamanoid
Nanocrystalline diamond

ABSTRACT

While graphene has held the center stage in nanocarbon material research since its isolation in 2004, less attention has been paid to nanometer-thick carbon films in which at least part of the carbon atoms are sp^3-hybridized, whatever the crystallographic structure. However, because of their composition, structure, physical and chemical properties, those nanomaterials exhibit competitive features that should be considered for the development of future sustainable technologies based on 2D materials. The purpose of this review is to provide a snapshot of the main advances in the synthesis of sub-10 nm thick sp^3-C-rich films, which include amorphous carbon hydrogenated or not, nanocrystalline diamond films, graphane, diamanes and diamanoids. Physical properties and applications (*i.e.* existing or potential) are also highlighted.

Glossary

1LG	single graphene sheet
2LG	bilayer graphene
a-C:H	hydrogenated amorphous carbon
AFM	atomic force microscopy
AGL	air-gap liner
ATR	attenuated total reflection
CCL	Cu capping layer
CVD	chemical vapor deposition
DB	low-k dielectric barrier
DECR	distributed electron cyclotron resonance
DLC	Diamond-Like Carbon
ECWR	electron cyclotron wave resonance
EELS	electron energy loss spectroscopy
ES	etch stop
FCVA	filtered cathodic vacuum arc deposition
FLG	few-layer graphene
FTIR	Fourier transform infrared spectroscopy
ga-C	graphenic amorphous carbon
ha-C	hexagonal amorphous carbon
HAMR	heat-assisted magnetic recording
HFCVD	hot filament CVD
HRTEM	high resolution TEM
IBD	ion beam deposition
ILD	intermetal and interlayer low-k dielectric
MAC	monolayer of sp^2-bonded amorphous carbon
MWCVD	microwave plasma CVD
NCD	nanocrystalline diamond
PBS	plasma bean source
PL	photoluminescence
PLC	polymer-like carbon
PLD	pulsed-laser deposition
PVD	physical vapor deposition
RF-PECVR	radio-frequency-plasma-enhanced CVD
SiV	silicon-vacancy
sp3C2D	sub-10 nm sp^3-C-rich carbon films, possibly hydrogenated
ta-C	tetrahedral amorphous carbon
ta-C:H	hydrogenated tetrahedral amorphous carbon
TEM	transmission electron microscopy
ULSI	ultra large scale integration
UNCD	ultrananocrystalline diamond
XPS	X-ray photoelectron spectroscopy
ZPL	zero-phonon line

* Corresponding author.
E-mail address: fpiazza@pucmm.edu.do (F. Piazza).

https://doi.org/10.1016/j.cartre.2022.100219

1. Introduction

Since graphene was able to be isolated in 2004 [1], it has been the subject of extensive research efforts to explore its exceptional physical properties, to improve the synthesis methods, and to develop a wide range of applications [2]. However, graphene suffers from the lack of an electronic bandgap [1]. This limitation has largely contributed to motivate the research on new 2D materials for electronic and optoelectronic applications [3] and has triggered the synthesis of a myriad of new materials, from mono-elemental ones (*i.e.* phosphorene [4], silicene [5]), to compounds such as boron nitride [6], F-diamane [7], transition metal dichalcogenides (TMDs) [8] and transition metal carbides, nitrides, or carbonitrides (MXenes) [9].

Sub-10 nm sp^3-C-rich carbon films, possibly hydrogenated, designated as sp3C2D in the following, have not attracted such a strong interest despite a set of promising features, which are either expected from the analogy with diamond or from calculations, or were revealed by experiments, including: *(i)* wide electronic bandgap; *(ii)* diamond-like mechanical properties; *(iii)* chemical inertness; *(iv)* biocompatibility; *(v)* mono-elemental composition (excluding the surface layers, which may be bonded to other elements such as hydrogen); *(vi)* they are based on one of the most abundant elements on Earth, which is compatible with sustainable development, and which could possibly favor the capture of the excess gaseous forms of carbon into materials in a double-winning strategy [10]; *(vii)* they are produced by physical or chemical vapor deposition (PVD or CVD) techniques compliant with the semiconductor industry.

This lack of interest may be partially explained by *(i)* the overall craze about graphene, which has hindered the potential interest of other 2D carbons, *(ii)* the eventual structural complexity of sp^3-C-rich materials which make them hard to characterize accurately, as shown, for instance, by the failure in providing unambiguous evidence of the synthesis of graphane (*i.e.* a sp^3-C layer obtained from the full hydrogenation of single-layer graphene) [11], and *(iii)* the difficulty in growing sub-10 nm nanocrystalline diamond films, as further detailed below. In 2018, it was considered that one remaining experimental challenge in carbon science was the development of a bulk synthesis method for 2D diamonds and that a "*real breakthrough would be to use CVD processes such as hot filament CVD in the presence of H_2 and CH_4, to yield scalable synthesis of 2D or 1D diamonds*" [12]. This was shortly followed by the successful synthesis of stable nanometer-thick and crystalline sp^3-bonded carbon sheets, including diamanes, diamanoids, and diamanoid/graphene hybrids, from the hydrogenation and conversion of graphene sheets exposed to a hot filament CVD-promoted hydrogenation process [13–17].

Because of the high potential of sp3C2D, the purpose of this review is to provide a snapshot of the main advances in their synthesis. Physical properties and applications are also highlighted. After the first section, which is devoted to a short presentation of the advantages and drawbacks of the most useful techniques for characterizing sp3C2D, we start with amorphous carbon for historical reasons. Nanocrystalline materials are then considered, starting with nanocrystalline diamond films, following with graphane, and then ending with diamanes and diamanoids for both respecting the chronology of research developments and addressing sp^3-C-based carbon films with incremental structural order. Although various elements can be incorporated in sp3C2D, this review will only consider hydrogen (H).

2. Structure-characterization techniques

Determining the sp^2-C/sp^3-C ratio, the hydrogen content, and crystallinity features if any is paramount for identifying the types of sp3C2D and discriminating between them. A review on common techniques to be used for this purpose can be found in Ref [18]. Because sp3C2D provides a very limited specimen volume, many of the techniques used in the case of thicker films are irrelevant, *e.g.*, nuclear magnetic resonance, combustion analysis, neutron and X-ray diffraction, analysis of the extended X-ray-absorption fine-structure (EXAFS), elastic recoil detection analysis. In this section, the advantages and drawbacks of the most useful techniques for characterizing sp3C2D, which are summarized in Table 1, will be briefly described for those interested in entering the field.

Table 1
The main characterization methods for sp3C2D materials.

Method	Info obtained	Limitations
XPS	sp^3/sp^2 ratio	H is not detected (contrary to N, O, F) Not shown to be usable in the case of hydrogenated amorphous carbon
Raman spectroscopy / microscopy Visible excitation	sp^2-C arrangements Mapping possible	sp^3-C are not directly detected in amorphous material Quantitative analysis is empirical
Raman spectroscopy / microscopy UV excitation	Similar sensitivity to sp^3-C and sp^2-C Mapping possible	Power must be carefully tuned to avoid any sample modification Quantitative analysis is empirical
IR spectroscopy / microscopy	C–H bonds Mapping possible	Only C bonded to H are detected Attenuated total reflection (ATR) mode damages the sample The absorption strength of the vibration modes is unknown for most of carbon materials
Electron diffraction	crystal structure	Specimen on TEM grid Some crystal structure cannot be discriminated May modify the sample – knock-on damage Local deformation may modify patterns
EELS	sp^3/sp^2 ratio Thickness (+/-20%) Dielectric constants	H is not detected Specimen on TEM grid May modify the sample Needs a reference sample

2.1. X-ray photoelectron spectroscopy

X-ray photoelectron spectroscopy (XPS) is a very sensitive surface technique but it cannot detect H. The kinetic energy of the emitted photoelectrons depends on the binding energy of the atomic orbital from which the electron originates. Because each element has a unique set of binding energies, XPS can be used to identify the elements within the escape depth of the photoelectrons in the near-surface region. Variations in the elemental binding energies (the chemical shifts) arise from the differences in the chemical potential and polarizability of the material. These chemical shifts can be used to identify the chemical state of the materials [19]. The ionization cross-sections for the XPS core level spectra are exclusively dependent on atomic factors and independent of the chemical state of the atoms when the energy of the X-ray photons is well above the absorption edge of the core level [20]. The intensity of the core-level peaks is then directly proportional to the density of atoms. There is a small shift of the C1s core level in the order of 0.9 eV between diamond and graphene [21]. Hence, Diaz *et al.* have shown that the C1s photoemission spectra of carbon in non-hydrogenated amorphous carbon films consist of two components arising from the sp^3- and sp^2-hybridized forms of car-

bon, which are chemically shifted by 0.9 ±0.1 eV from each other [21]. Therefore, XPS provides a straightforward way to determine the relative concentrations of sp^3-C and sp^2-C in non-hydrogenated amorphous carbon films by decomposing the C1s photoemission spectra into those two lines, with no need for a reference sample as in the case of electron energy loss spectroscopy (EELS) [21]. This method was then extrapolated to hydrogenated amorphous carbon films without any validation. However, fitting the symmetrical C1s spectra of most of hydrogenated amorphous carbon films remains ambiguous. In the case of a series of monodisperse polystyrene/polyethylene tapered block copolymers, with known sp^2-C/sp^3-C ratios, Turgeon and Paynter showed that the C1s peak exhibited no significant shape variation as the sp^2-C concentration was varied [22].

2.2. Raman spectroscopy

Raman spectroscopy is the most widely used technique for the characterization of phonon modes in carbon films. The technique detects the small portion of scattered photons from the incoming laser beam which are subjected to a loss of energy, hence a change in their frequency, during their interaction (so-called inelastic) with the phonons from the material investigated. Most carbon materials exhibit characteristic spectra [23]. In graphene, which is used as precursor for graphane, diamanes or diamanoids as detailed below, the intensity ratio of the D and D' defect-activated peaks, $I_D/I_{D'}$, is used to get information on the nature of defects [24]. $I_D/I_{D'}$ is maximum (∼13) for sp^3-defects [24], it decreases down to ∼9 for loop defects [25], then it decreases further for vacancy-like defects (∼7) and for boundaries (∼3.5) [24], and may reach minimum values (below 2) when the nature of defects generates polarization effects [26]. Raman scattering from sp^2-C is a resonant process for visible wavelength excitation and results in a 50 to 230-fold signal enhancement relative to that of non-resonant sp^3-C Raman scattering [27]; thus, it is necessary to employ UV excitation to obtain a more evenly weighted probing of sp^3-C and sp^2-C sites. However, UV Raman measurements are prone to damage high-energy chemical systems, such as hydrogenated carbon films. The exposure time and power must be carefully tuned to avoid any structure modification. Empirical analyses are employed to estimate sp^3-C fraction, sp^2-C clustering, and hydrogen content [23,28].

2.3. Infrared spectroscopy

IR spectroscopy is the measurement of the wavelength and intensity of the absorption of infrared light by the material molecular vibrations. It can be used to detect hydrogen and to qualitatively study C–H bonding from the analysis of the C–H stretching-vibrational mode bands at 2800–3300 cm^{-1} [29]. The infrared response is complementary to the visible Raman one and less sensitive to electronic effects [30]. In the case of hydrogenated amorphous carbon, efforts were made to quantitatively determine the sp^2-C/sp^3-C ratio and the total amount of H atoms from the fitting of the C–H stretching band with Gaussians. However, this approach faces the following challenges: *(i)* the position and width of the nine sub-bands corresponding to the nine possible vibration modes, can vary depending on the structure [29] and fitting may be ambiguous as multiple solutions can be obtained; *(ii)* the absorption strength of each vibrational mode must be considered. Hence, if they are known in the case of free molecules [31], they are unknown for most of carbon materials. In the case of free molecules, the absorption strength varies significantly throughout the various modes. The absorption strength for the sp^3-C–H stretching mode is nearly 32 times lower than the corresponding value for the sp^3-C–sp^3-C–H_3 stretching mode [31]; *(iii)* it does not take into account any hydrogen not bounded to a carbon, nor any carbon not bonded to a hydrogen. Therefore, the estimation of both the sp^2-C/sp^3-C ratio and the total amount of H can be erroneous.

2.4. Electron diffraction

When a coherent electron beam is scattered elastically by a periodic material such as a crystal, the scattering occurs according to Bragg's law in specific directions of space, and the electron diffraction pattern of the crystal is obtained [32]. As amorphous carbons are not periodic, it could be thought that electron diffraction is useless for studying them. However, some periodicity is always present, such the C–C bond length, or others. Hence, the method can be used to study amorphous carbon films as well, or merely discriminate between amorphous and crystalline structure for the least. In the latter case, the determination of the structure may be possible from characteristic patterns. Attention has to be paid, however, that electron beams can be highly energetics, hence likely to alter the original structure. For instance, carbon atoms involved in graphene lattice may be knocked-off by incoming electrons with energy higher than ∼86 keV [33], and materials involving C–H bonds may be even more sensitive [17,34] because of the low Z number of H [35]. On the other hand, using very low-energy electrons, down to 5 keV, may be quite useful to reveal the type of stacking sequences in 2D graphenes and/or the number of layers involved [35], which is important for their conversion into diamane or diamanoid as discussed below. However, attention has to be paid that local deformations may modify the patterns, in particular spot intensities, and make difficult such an analysis [15].

2.5. Electron energy loss spectroscopy

EELS uses the fact that some of the electrons from an electron beam passing through a film can be inelastically scattered by the inner (core–shell) sample electrons producing ionization edges that are characteristic of specific elements. The high-energy loss region at the C1s (K edge) at 284 eV can be compared to reference spectra such as those from diamond and graphite [36], and has been used to estimate the sp^3-C fraction in amorphous carbon. The near edge consists of two features, a peak at 284 eV due to the excitation to π^* states of sp^2-C, and a step at 290 eV due to the excitation of sp^3-C and sp^2-C sites to σ^* states. As diamond has no peak at 284 eV, the sp^2-C fraction of a carbon film can be found by taking the area ratio of the 284 over the 290 eV step within some energy window, and comparing it to the ratio for a 100 % sp^2-C reference sample that has to be isotropic in the orientation of its π bonds [37]. As with electron diffraction, attention has to be paid to the same risk of structural damages induced by the electron beam.

3. Sub-10 nm thick amorphous carbon films

3.1. Classification

It can be considered that the research on amorphous carbon, initiated 60 years ago with the study of evaporated carbon film [38,39], experienced a turning point with the synthesis of ion beam deposited film [40] and is nowadays very mature. Numerous and extensive review papers are available, such as Robertson's [41], although most of the research concerns films whose thickness is higher than 100 nm. Compared to such thick films, ultrathin films are likely to exhibit specific physical and chemical properties. For instance, electronic properties may be more dependent on a higher proportion of surface atoms. The interface and surface regions, which may exhibit a distinct hybridization ratio (see discussion below), may also have a stronger impact on physical properties.

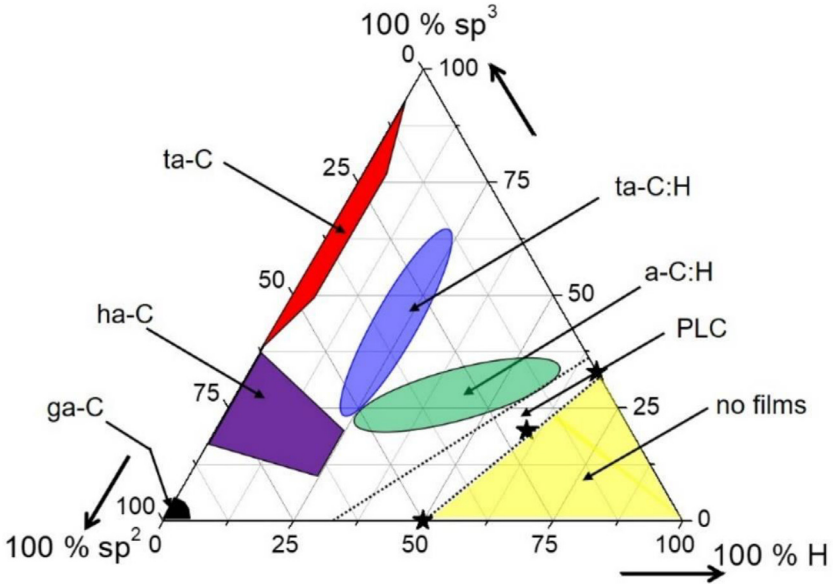

Fig. 1. Ternary phase diagram for amorphous carbons, based on the original work by Jacob and Möller [42], subsequently modified by Roberston [41], and then by us (see text). In the labels, the letters "*a*", "*t*", "*h*" and "g" stand for "amorphous", "tetrahedral", "hexagonal" and "graphenic", respectively. PLC stands for polymer-like carbon. The diagram is valid for both thick and thin films, keeping in mind that other important features are not considered in the diagram, such as the possible variation in hybridization across the film thickness in the case of sub-10 nm films (see text). The domain frontiers are indicative.

Amorphous carbons are most often composed of carbon (both sp^3-C and sp^2-C) and hydrogen, although it is possible to produce hydrogen-free films [42]. Other elements can be incorporated such as N, P, Si, F, or various metals (*e.g.* Cu, Ag, or Al), but those variants are out of the scope of this review. Because physical properties depend primarily on both the structural and chemical compositions, a ternary phase diagram was introduced by Jacob and Möller [42] and then subsequently completed by Robertson [41] to compare published data. Initially built based on thick films, this diagram remains useful for the sub-10 nm-thick films targeted in this paper. However, we propose a further modified version of it as Fig. 1, which revisits a bit part of the nomenclature proposed in [41].

The shaded area (yellow in the colored version) in Fig. 1, close to the hydrogen-rich corner, corresponds to the region where no stable film can form [42]. This region is limited by the line of the existence of long-chain polymers such as polyethylene (67 at.% H, 33 at.% sp^3–C), polybutadiene (60 at.% H, 20 at.% sp^3–C, 20 at.% sp^2–C) and polyacetylene (50 at.% H, 50 at.% sp^2–C). Those three polymers are indicated by using black stars in Fig. 1.

Fig. 1, actually, appears not to be ideal. There are many forms of amorphous carbon films which discriminate from their composition indeed, but also from other features which should be added to the ternary phase diagram as additional dimensions, for instance: the variations in hybridization states across the film thickness (see discussion below) [41]; whether sp^2-C is either in alkene (chains) or aromatic forms and in which proportions; whether carbon atoms of same hybridization state gather into clusters, and of which dimensions. Reporting this additional information into a single diagram appears to be difficult, but the related features have to be kept in mind, as they are likely to generate materials with different behavior and properties while located at the same place in the diagram.

The phase diagram in Fig. 1 is compositional, *i.e.*, it is independent of the synthesis process. However, because most of the materials from which the phase diagram was built were obtained by a process involving ion bombardment, correspondence was made between the bonding and properties of the various amorphous carbon films and the energy of the impinging carbon ions during the growth process (see section 3.1.2). However, amorphous carbon films may now be prepared by a variety of methods. Therefore, despite the classification proposed in [41] has been widely accepted, some amendments are needed, as introduced below:

- Films such as those prepared by low energy ion bombardment have large hydrogen (40–50 at.%) and sp^3-C (up to 60 at.%) contents. These films are called ***polymer-like carbons*** (***PLC***) as most of the bonds involving sp^3-C are C–H bonds. They are mechanically soft and have low mass-density (typically 1.2 to 1.6 g/cm^3). According to Fig. 1, PLC with high sp^2-C and low sp^3-C are expected, but they have not been investigated experimentally in detail because the focus has mainly been on sp^3-C-rich films.
- When the hydrogen content drops (~30–50 at.%) while the sp^3-C content is between 20 and 40 at.%), as for films prepared with intermediate energy ion bombardment, the films are mechanically harder and have higher mass-density since cross-linking between sp^3-C is higher as compared to PLC. Films are of the ***hydrogenated amorphous carbon*** (***a-C:H***) type.
- When the sp^3-C content becomes very high (~70–85 at.%) and the hydrogen content is decreased down to ~20–30 at.%, the films are designated as ***hydrogenated tetrahedral amorphous carbon*** (***ta-C:H***) as suggested in [43]. They are hard and their mass-density reaches 2.4 g/cm^3. If the synthesis is carried out without the presence of hydrogen, the films are designated as ***tetrahedral amorphous carbon*** (***ta-C***) as proposed in [44]. Their mass-density can reach 3.1 g/cm^3 [41]. ***Ta-C and ta-C:H*** have attracted great practical interest because the high fraction of bonds between sp^3-C confers many of the beneficial properties of genuine diamond while being synthesized at lower substrate temperature. Indeed, they can be grown at near room temperature with a reasonable growth rate (typically 0.83 Å/s) [41], while diamond typically requires substrate temperatures higher than 400 °C [45,46]. As a counter-example, the growth of nanocrystalline diamond on plastic substrates at a lower temperature (below 100 °C) was achieved, but growth rates are too low for practical applications (below 0.17 Å/s) [47–49].

- If the sp^3-C fraction is below ~40 at.% along with a limited amount of H (< 25 at.%), the related amorphous carbons were once designated as "sputtered a-C(:H)" to refer to its commonly used synthesis method [41], or "graphite-like" [50]. We propose to substitute those two designations because they both present some inconvenient. The first one is because it refers to a specific synthesis method while other methods can be used to obtain the same composition. The second one is not appropriate either, because the crystallographic structure has nothing to do with that of graphite. Indeed, the materials reported in the phase diagram should be amorphous, *i.e.* built with usually very-small-size graphenes with severe distortions combined with a high amount of various kinds of in-plane defects which prevent the graphenic entities to pile-up. As soon as graphenes, even sub-nanometer-large (as in the basic structural unit (BSU) model introduced by Oberlin [51]), are able to stack by a minimum of two, a crystallographic structure is obtained, that is, the turbostratic structure. In such sp^2-C-rich materials, the orientation of the graphene stacks is random, making the material isotropic in terms of texture and properties. As a logical counterpart to the *ta-C* carbon type above-described, we propose to designate those sp^2-C-rich materials as ***hexagonal amorphous carbon*** (***ha-C***), where *h* stands for “hexagonal”.
- When the hydrogen content drops further down to 0 or close and the hybridization becomes mainly sp^2, as obtained at high energy ion bombardment, the films were referred to once as "glassy carbons" and "graphitic C" [41], or "graphitic-like carbon" (*GLC*). Although the sp^2-hybridization prevails in those materials, they always exhibit some sp^3-hybridization character, coming from sp^3-C atoms at the grain boundaries or from sp^2-C for which C–C bonds are no longer planar (as in fullerenes for instance, for which all the carbon atoms are supposed to be sp^2-hybridized, but they all exhibit 30 % of the sp^3-hybridization character due to the lattice curvature needed to close the molecule [52]). As in the case of *ha-C*, the crystallographic structure of those materials has nothing to do with that of graphite for the same argument. In such materials, the orientation of the graphene stacks is random, making the material isotropic in terms of texture and properties. This isotropic feature made some of these materials designated as "glassy carbons", because of their glass-like behavior, but then they may no longer be described as amorphous as long as they exhibit stacked graphenes, whatever their dimensions, and should not belong to the phase diagram of Fig. 1. For those exhibiting a genuine amorphous character, *i.e.*, an absence of periodicity even at a short distance, thanks to the term "graphenic" recently introduced [53], it is more relevant to designate them as ***graphenic amorphous carbon*** (***ga-C***), where *g* stands for “graphenic”. It is therefore necessary to investigate in detail, at the nanoscale, using transmission electron microscopy (TEM) techniques, whether such materials are all amorphous. This is behind the scope of the present review. As a particular example of *ga-C*, recently, a uniform and stable **monolayer** of sp^2-bonded **amorphous carbon** films (***MAC***) was obtained by a laser-assisted CVD growth process at substrate temperature as low as 200 °C [54]. Atomic-resolution TEM characterization (beam current of about 20 pA; energy of 60 keV) unambiguously showed the complete absence of long-range periodicity and a structure formed by nanometer-sized, randomly oriented, and strained sp^2-C clusters comprising of five, six or seven-member rings embedded in a continuous random network [54]. The 2D band, which is of high relative intensity in graphene, is not observed in Raman spectra, which display separated but overlapping D and G bands which is characteristic of disordered graphenic material [54]. C1s XPS spectra show that the bonding is mainly between sp^2-C [54]. Considering the phase diagram of amorphous carbon (Fig. 1), the synthesis of this type of *MAC* (better designated as *g-MAC*, to follow the logic of Fig. 1’s nomenclature) could open the door to the elaboration of a wide range of *MACs* which would include an increasing proportion of sp^3-C, hence subsequently designated as *h-MAC*, and then *t-MAC* (in that case, the "monolayer" character would refer to the layer of carbon atoms only, as H atoms located above and below this layer would be necessary to saturate the sp^3-hybridized ones.

It is worth noting that the term ***Diamond-Like Carbon*** (***DLC***) [41] is not present in Fig. 1, although it is widely used in the literature to designate amorphous carbon films, hydrogenated or not. This is because it is a poor designation, considering how far the material is from genuine diamond because of its hydrogen content and its amorphous structure. Of course, the term is justified by the fact that some of the physical properties of diamond are shared with amorphous carbon films, hence using it is acceptable. However, which types of materials *DLC* is supposed to stand for is fuzzy, as it is used to designate amorphous carbon films as soon as the sp^3-C content is sufficiently high, whilst which sp^3-C content this means is never mentioned. Therefore, "*DLC*" should only be used as a generic term, roughly gathering the three sp^3-rich film areas *ta-C, ta-C:H* and *a-C:H* in Fig. 1.

In the case of sub-10 nm films elaborated from an ion-assisted method such as the filtered cathodic vacuum arc deposition (FCVA) or the pulsed-laser deposition (PLD) processes (see Section 3.2), the material classification according to the phase diagram displayed in Fig. 1 is challenged by the resulting layered structure obtained, as evidenced in [55,56]. High-resolution TEM (HRTEM) image contrast revealed distinct layers of different mass-densities within a given film. Overall, every film exhibits interfacial, bulk, and surface regions. The thicknesses of the interfacial and surface regions increase with deposition energy and are less dense than the bulk layer. In the case of PLD deposited ta-C, depending on the deposition energy, the thickness of the interface region varies between around 2 and 8 nm, while the surface layer can extend over nearly 10 nm [55]. In the case of FCVA-deposited *ta-C*, when the carbon ion energy is increased from 10 to 330 eV, the thickness of the interface and surface regions varies from 2 to 15 nm and from 10 to 25 nm, respectively [56]. In this case, it is not clear which sp^3-C fraction needs to be considered for positioning the corresponding film into the phase diagram, *i.e.*, either the value corresponding to the “bulk” or that corresponding to the mean value across the whole film thickness.

The deposition of sub-5-nm thick amorphous carbon films under optimal FCVA working conditions (see Section 3.2), is therefore challenging because the thickness of the highly sp^3-hybridized bulk layer becomes comparable with the thickness of the interfacial and surface layers, which are richer in sp^2-C. For the bulk layer to form, film growth must exceed the interface layer. Thus, without the formation of a sufficiently thick bulk layer with relatively high sp^3-C content, further film thinning cannot be achieved by simply decreasing the deposition time if the structural integrity of the film is to be preserved. Therefore, to further decrease the film thickness, efforts must be directed toward minimizing the thickness of the sp^2-C-rich interface and surface layers, while maintaining the prevalence of the sp^3-C-rich bulk layer. A possible method is to use a large ion incidence angle and/or low substrate bias voltage during initial deposition to decrease the interface layer thickness, switching later to a small ion incidence angle and/or high substrate voltage to generate deposition conditions promoting sp^3 hybridization, as in [57]. Following such a method, the growth of 1−4-nm-thick amorphous carbon films with a sufficiently thick bulk layer with high sp^3-C content (around 50–60 at%) was achieved [57].

An alternative is a use of a synthesis method that does not use any ion bombardment during the film formation. Recently a new method for preparing a conformal amorphous carbon layer with a thickness of 1 nm was shown [58]. In this method, a polystyrene brush of uniform thickness which was grafted onto SiO_2/Si substrate was transformed into ultrathin amorphous carbon layer without pinholes or hillocks by UV crosslinking and subsequent carbonization. However, as revealed by XPS C1s and Raman spectra, and by surface roughness analysis, the films produced are sp^2-C-rich rather than sp^3-C-rich [58].

3.2. Synthesis

The methods used to synthesize sub-10 nm sp^3-C-rich amorphous carbon films are similar to those used in the case of thicker films. A wide range of methods have been developed [41]. The common feature of those methods is that films are obtained by ion beam deposition (IBD), *i.e.*, they are condensed from an ion beam containing medium energy carbon (~100 eV) or hydrocarbon ions. *ta-C* and *ta-C:H* are elaborated from methods which can provide a carbon ion flux at about 100 eV per carbon atom, with a narrow energy distribution, a single energetic species and a minimum number of non-energetic ones (generally neutral) [41]. Until recently, there was a consensus regarding the mechanism promoting sp^3-bonding between carbon, which was designated as the subplantation model [59–61]. Recently, it was shown, using molecular dynamics simulations based on machine-learned interatomic potential trained from density-functional theory data, that the so-called "peening" model is the dominant mechanism responsible for the high sp^3-C content [62]. It was shown that pressure waves lead to bond rearrangement away from the impact site of the incident ion, and high sp^3-C fraction arises from a balance of transitions between sp^2-C and sp^3-C [62]. Also, for constant ion energy, the proportion of sp^3-bonding between carbon atoms can be increased by increasing the ion flux above $\sim 2 \times 10^{15}$ ions cm^{-2} s^{-1} [63]. This was interpreted in terms of the propagation and/or interference of shock waves generated by ion impacts during the growth [63,64].

ta-C is deposited by mass-selected ion beam, FCVA or PLD [55,65–70]. FCVA is more advantageous than PLD because it uses narrower distributions of charge, cluster size, and energy [71].

ta-C:H is obtained by high plasma density techniques from a hydrocarbon precursor, such as the Plasma Beam Source (PBS) [72], Electron Cyclotron Wave Resonance source (ECWR) [73,74], and Distributed Electron Cyclotron Resonance (DECR) [63,64,75,76]. The maximum reported sp^3-content is 75% [72,77] which goes along with the highest Young modulus of 300 GPa [78], and a maximum mass-density of ~2.4–2.5 g/cm^3 [63,75–78]. Early claims for a mass-density of up to 2.9 g/cm^3 for *ta-C:H* [72,73] were overestimated, due to an incorrect choice of the electron effective mass for mass-density evaluation via EELS. With the correct electron effective mass, the mass-density value becomes 2.4 g/cm^3 [77]. Hydrogen content varies between 20 and 30 at.%. *a-C:H* deposited by standard radio-frequency-plasma-enhanced CVD (RF-PECVD) does not achieve such properties [41,79–82], due to the low degree of ionization of the deposition flux, and dispersion of the ion energy. When compared with *ta-C, ta-C:H* has the advantage of being deposited without any contamination from submicron-size particles bouncing off the walls, which are difficult to avoid in FCVA-deposited *ta-C* [83].

3.3. Properties and Applications

Whatever their thickness, the properties of *ta-C:H* and *ta-C* resemble that of diamond, that is, including high hardness and high Young modulus, low friction coefficient, high wear resistance, smoothness, optical transparency in a wide range of wavelengths, chemical and biological inertness, low electron affinity, high electrical resistance and lack of magnetic response [41]. Therefore, these films are competitive engineering materials for cost-effective hard coating and have been used in widespread applications, primarily as protective coatings in areas such as magnetic [84] and optical storage disks [85–87], optical windows and medical implants, or in micro-electromechanical devices [41]. The sp^3-C content alone mainly controls the elastic constants, but films with similar sp^3-C and hydrogen contents but different sp^2-C arrangements (*e.g.* clusters or chains) can have different optical and electronic properties [41]. Most applications deal with rather thick films (at least several tenths of nanometers). However, some applications require few-nanometer-thick films. This is the case of the following two: (i) protective coating for ultrahigh-density data storage in magnetic disks; (ii) low-dielectric constant film for microchips. We will review these two applications below.

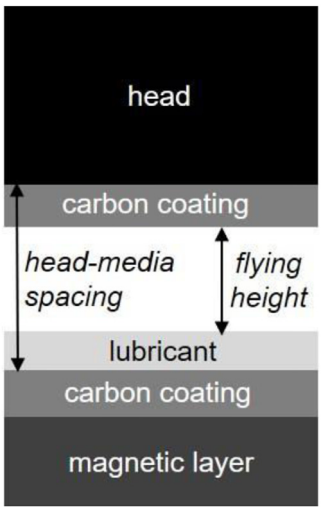

Fg. 2. Schematic of head-media spacing components in a hard-drive-disk device.

3.3.1. Protective coating for magnetic storage

In hard disk, the data are stored in a thin cobalt-based magnetic layer. A coating of amorphous carbon is deposited over this magnetic layer to protect it against wear (originally) and above all, corrosion (Fig. 2) [88]. A thin layer of perfluoropolyether compound (one or two monolayers), which is deposited on the carbon coating, serves as a lubricant [88]. A read/write head, which is also protected by an amorphous carbon coating, flies above the rotating disk on an aerodynamic bearing (Fig. 2) [88]. Basically, the fundamental corrosion mechanism involves the following two reactions: *(i)* $Co = Co^{++} + 2\ e^-$ (oxidation reaction); *(ii)* $2\ H_2O + O_2 + 4\ e^- = 4\ OH^-$ (reduction reaction) [89]. For those two reactions to take place, the environment must have direct access to the magnetic media and an electronic path must facilitate charge transfer. If either of these two conditions is substantially suppressed, the media corrosion is effectively suppressed [90].

Until very recently, there was no competing material to amorphous carbon. At the beginning, the chemical inertness, lack of grain boundaries, and excellent topographical conformity made *ta-C*, as obtained by magnetron sputtering, for instance, an appropriate corrosion barrier [91]. Later, *a-C:H*, which was produced by the reactive sputtering in $Ar+H_2$ atmosphere, was used to enhance the electrical resistance [92], and to provide protection against mechanical wear and damage during head crashes [41]. Besides, hydrogen improved the interaction with the lubricant [93]. The increase in magnetic recording areal density has required the decrease of the distance between the read/write head and the

magnetic media, and therefore the decrease of the carbon coating thickness (on both the disk and the head) (Fig. 2) [90]. As its thickness was decreased, the mass-density of such thin sputtered amorphous carbon film became too low (1.5–1.7 g/cm^3) to achieve pin-hole-free coverage, which is necessary to protect the disk against corrosion [90]. Therefore, denser films (*ta-C* and *ta-C:H*, with higher sp^3-C content and hardness), which were obtained from more energetic processes (IBD, FCVA, and PECVD other than RF-PECVD such as ECWR and ECR), needed to be used [90]. It has been necessary to carefully tune the energy of the carbon atoms from the impinging ions to reach sufficiently high mass-density while avoiding a loss in magnetic properties of the magnetic layer or an enhancement of corrosion through Co atoms backscattered closer to the top surface of the carbon layer (*i.e.*, interlayer mixing) [90]. Currently, to reach ∼1 Tb/in^2 areal density, ∼2.5 nm-thick PECVD-grown *a-C:H* coatings are used on commercial disks (mass-density of ∼2.1 g/cm^3; hydrogen content of ∼40 at.%) [94] while ∼2.7-nm thick FCVA-deposited *ta-C* films are used on the heads (mass-density of 3.0 g/cm^3) [95]. Based on industry roadmaps, the average carbon coating thickness should be reduced down to ∼1.6 nm to achieve an areal density of 4 Tb/in^2 [96]. However, the reduction of the thickness below 2 nm may introduce many challenges regarding the resulting tribology and corrosion resistance [97]. Besides, as the hard-drive-disk industry moves towards the introduction of heat-assisted magnetic recording (HAMR) technology, the disk coating must withstand high recording temperature, above 500 °C. This is too high for *a-C:H*, as commercially used *a-C:H* films exhibit thermal stability up to a maximum temperature in the range of 400–450 °C [94]. Heating above this critical temperature leads to hydrogen depletion and sp^2-C clustering [94]. Better thermal stability was reported in FCVA-deposited *ta-C* under laser irradiation in HAMR-like conditions [98]. However, FCVA-deposited *ta-C* are not used as disk overcoat yet due to the presence of sub-micron-size carbon particles from the graphite source [83,96]. Further research and development in tribological materials for both heads and media are needed to enable HAMR technology. Recently, graphene-based overcoats were proposed as an alternative to amorphous carbon [99].

3.3.2. Low k -constant dielectric material for back-end processes

Amorphous carbon has been considered as low dielectric constant material for Ultra Large Scale Integration (ULSI). One of the priorities to both sustain Moore's law (*i.e.* "More Moore") [100] and "More than Moore" dimensional scaling [101,102] is to improve the performance of nano-electronic metal-interconnect structures by using insulating dielectrics with ever lower values of dielectric permittivity (k) [103]. Those materials are the intermetal and interlayer low-k dielectrics (ILD), the air-gap liner (AGL), low-k dielectric barriers (DB), etch stops (ES), and/or Cu capping layers (CCL) [103,104]. The purpose of ILD/AGL materials is only to electrically isolate adjacent metal lines, while there are more requirements on DB/ES/CCL materials (*e.g.* electrical, mechanical, thermal, electromigration) [103]. Robust DB/ES/CCL films with either reduced dielectric constant ($k < 4$) and/or which exhibit robust diffusion barrier performance at thickness < 2 nm, which is the current International Technology Roadmap for Semiconductors (ITRS) forecast, are required [103]. In the case of ILD and AGL materials, k must decrease below 2.3 and 4, respectively [104]. New materials need to be identified and examined [103]. One of the most attractive options is C-lattice-based materials, even if few investigations of pure carbon materials have been reported [103]. Diamond films exhibit a high mass-density (3–3.5 g/cm^3) and many excellent physical properties [105] with a relatively low k of ∼5.7 [106], but conventional synthesis conditions are not suitable for metal-interconnect applications because of the too high substrate temperature [103]. Hydrogenated amorphous carbon films can be deposited at near room-temperature and can reach k values down to 2.6 if of the *PLC* type [41]. However, *PLCs* have low thermal stability, below 400 °C [107]. Only films with k above 3.3 were shown to be sufficiently stable [107]. Most hydrogenated amorphous carbon materials investigated for metal-interconnect applications have been targeted for low-k ILD or planarization applications [103,107]. However, the Cu diffusion resistance of a *PLC* film with a $k = 2.7$ was reported after annealing at 450 °C for 1 h [108]. One issue with hydrogenated amorphous carbon films to be used for low-k ILD/DB/ES applications is the typically low resistivity values reported [103], which were attributed to conductive sp^2-C (polyaromatic) clusters in the matrix material [41]. However, the formation of the latter can be minimized and hydrogenated amorphous carbon films with low-k (< 2.5) and high breakdown strength (8 MV/cm) were achieved [109]. Those results are very promising considering the multiple possible structure configurations offered by the phase diagram of amorphous carbon materials (Fig. 1). However, ultimately, the thermal conductivity of amorphous carbon films (hydrogenated or not), which is increasingly needed for power dissipation, will be low (∼0.2–3.5 W/m.K) [110].

4. sub-10 nm thick nanocrystalline diamond films

4.1. Synthesis

The research on nanocrystalline diamond (*NCD*) films was initiated 30 years ago and is now well advanced [111]. Numerous review papers covering all the corresponding fundamental aspects (*i.e.* structure, synthesis, properties, and applications) are available, such as by Butler and Sumant [111]. *NCD* films of the highest quality (*e.g.* crystallinity and sp^3-bonded carbon fraction) can be divided into two broad categories, both grown by microwave plasma CVD (MWCVD) or hot filament CVD (HFCVD) [111] at low pressure (typically several tens of Torr), but differing by both the film microstructure and growth chemistry [111]:

(i) The *NCD* films are typically grown in hydrogen-rich and carbon-lean CVD growth atmospheres (typically less than 2 at.% of CH_4 in H_2). They are polycrystalline films, with the grain size varying with nucleation density and thickness, but is typically within the range of 5–100 nm. The amount of sp^2-bonded carbon trapped at defects or grain boundaries can be very low (< 0.1% for the highest quality) [111].

(ii) The so-called ultrananocrystalline diamond (*UNCD*) films, are typically grown in argon-rich, hydrogen-poor CVD atmospheres. Grain size and sp^2-bonded grain-boundary width are typically within the range of 2–5 nm and 0.6–4 nm, respectively, so the sp^2 fraction is typically between 2 and 5 at.% [112–115]. During *UNCD* growth, the secondary nucleation is active and generates densely-packed UNCD grains [111]. The first growth of *UNCD* films was reported in 1994 [112] but the *UNCD* denomination is used since 2001 [116].

Most reports deal with rather thick films (thickness above 100 nm). This is closely related to the high surface energy of diamond and its initial growth mechanism. The large surface energy difference between diamond and most non-diamond substrates complicates the growth of diamond on those substrates [117]. The initial growth follows the Volmer-Weber model (*i.e.* 3D growth of isolated islands), so that the nucleation density (*i.e.* the number of grown nuclei per surface area) is low [118]. A nucleation-density enhancement step, also called seeding, is needed [118]. The minimum thickness for getting pinhole-free coalesced films is highly dependent on the nucleation density and the size of the nuclei [118,119]. When conventional growth is applied (nucleation density below around 4×10^{10}.cm^{-2}), a thickness of at least 100 nm is necessary to achieve a continuous diamond film on a non-diamond

substrate [119]. To synthesize thinner homogeneous pinhole-free films, nucleation density must be increased [119]. A lot of work has been done to increase nucleation density, initially to avoid voids at the interface between the film and the substrate during film coalescence, which may threaten adhesion and degrade thermal conductivity at the interface [120]. After coalescence is achieved, the diamond crystals underneath the coalesced film do not grow anymore, so the voids at the interface remain present. Two reviews on diamond nucleation on heterogeneous substrates were recently published by Mandal [118] and by Handschuh-Wang et al. [121], the latter being specific to films with thickness below 100 nm. The detailed theory of diamond nucleation can be found in [122]. Among the various methods developed to increase nucleation density, only the electrostatic self-assembly seeding and the chemical nucleation will be considered here. The former method, which has been investigated in the past 10-years, is the only current route leading to the synthesis of sub-10 nm films [121] while the latter appears as a promising approach to elaborate even thinner films. The electrostatic self-assembly seeding method is a refinement of the abrasion seeding process where diamond particles in an ultrasonic bath generate nucleation sites on the substrate by abrasion [121]. The reduction of the particle size leads to the increase of both the seeding and nucleation densities, and consequently to the synthesis of sub-100 nm diamond films. In 2011, a significant milestone was reached when a void-free, mirror-smooth, and 30-nm thick *UNCD* film was elaborated from a seeding density of $8 \times 10^{11}.cm^{-2}$ obtained from 4 nm-sized, disaggregated diamond nanoparticles [123]. Before that breakthrough, only diamond particle agglomerates of around 200 nm in size were operating during the seeding process because of the high resistance of the diamond nanoparticles against deagglomeration [121]. In [123], the seed density variation according to various substrate pretreatments and types of the seed powders was attributed to the variation in the relative zeta potential values of the substrates and seed powders, indicating the coulombic nature of the seeding process [123]. The variation of the surface zeta potentials was attributed to the surface terminations induced by the respective pretreatments. It became clear that the adsorption and self-assembling of diamond particles with high density and homogeneity from seeding slurry was obtained from the electrostatic interactions between the nanoparticles and the substrate surface [121]. The CVD conditions used in [123] ensured active secondary nucleation that generated densely packed *UNCD* grains. The agglomeration of the nanoparticles in the slurry is avoided by tuning the zeta potential of the particles to an absolute value over 30 mV or by using steric hindrance obtained from small molecules or surfactants [121,124]. Electrostatic self-assembly is achieved by the antipodal charge of the substrate surface (*i.e.* negative) and the stabilized particles (positive) [121]. The zeta potential of the particles can be tuned by the pH, the addition of a stabilizing agent and change of its concentration, the ionic strength, and the type of solvent [121]. The charge of the substrate can be varied by interlayer deposition (*e.g.*, a charged polymer) [125]. The zeta potential optimization approach was refined in 2017 by Stehlik et al., to tune the thickness of synthesized *NCD* films down to values as thin as 5.5 nm (Fig. 3a) [126]. On the one hand, the seed particle size was further reduced down to 2 nm by air oxidation, and on the other hand, a sophisticated colloidal chemistry approach, leading to zeta potential optimization, was employed. A positive zeta potential reaching the colloidal stability region of the 2 nm hydrogenated diamond nanoparticles enabled the formation of homogeneous, extremely dense in nuclei ($1.3 \times 10^{13}.cm^{-2}$), thin (2 nm), and smooth (RMS $<$ 0.8 nm) nucleation layers on Si/SiO_x substrates from aqueous (deionized or 10^{-3} M KCl-based) colloids.

It may be possible to further decrease the film thickness below 5 nm by further decreasing the seed particle size and increasing the nucleation density. In this sense, chemical nucleation, using adamantine ($C_{10}H_{16}$), the smallest unit cage structure of the diamond crystal lattice, or variants (*i.e.* diamondoids), is a promising approach [121]. However, the low melting and low sublimation temperatures of those molecules require special immobilization procedures and growth parameters (*i.e.* low substrate temperature) [121]. The highest nucleation density thus far ($6 \times 10^{11}.cm^{-2}$) was achieved by chemically bonded 2,2-divinyladamantane on silicon as nucleation sites and subsequent sequential incubation, comprising of low-power-density plasma to facilitate the formation of diamond nucleation sites, and a growth phase [127].

4.2. Applications

Sub-10 nm thick *NCD* films are of great interest for a wide range of applications such as microelectromechanical and nanoelectromechanical devices [128], coating for packaging of implantable electronic devices [129] including biosensors [130], coating for optical devices with high transparency from UV to IR or functional material for transparent electrodes [131–135], conductive and transparent coating for solar cells [136,137], and flexible electronics [138]. The only application that has been experimentally explored in the case of sub-10 nm thick films is as host material of color centers for solid-state single photon emission to be used in a wide range of applications such as quantum computers and cryptography, magnetometers to substitute GPS systems and implantable biosensors [126,139,140]. Therefore, the main corresponding results obtained will be summarized below. As compared to the extensively studied nitrogen-vacancy with a broad emission spectrum at room temperature [139], the SiV centers exhibit a narrow room-temperature zero-phonon line (ZPL) at around 739 nm, in which 70% of its PL is concentrated [141,142]. Very thin *NCD* films are of great interest as they offer the opportunity to place a high density of SiV centers that act as sensors, near the film surface, which is important to obtain a good response to any surrounding environment change. SiV centers can be directly incorporated into the diamond lattice during the CVD process from a Si substrate or from another Si source located near the plasma [143]. PL from SiV centers at 739 nm from 5–6 nm thick *NCD* films was recently reported [126] (Fig. 3b). The SiV PL signal came on average from 3.5 nm-large SiV-doped diamond nanocrystals. The absolute PL intensity of the SiV center peak was shown to increase with diamond thickness (Fig. 3b). It was also shown to be sensitive to surface termination. All the as-grown films exhibited lower PL intensity than after a relatively mild surface oxidation treatment (450 °C, 30 min) (Fig. 3b). There was no change in the thickness, morphology and Raman spectra after the oxidation treatment. The increase of the SiV PL intensity after the oxidation treatment was supposed to be due to changing from hydrogen to oxygen surface termination [126]. This is consistent with an observed positive effect of the oxygen surface termination on the SiV PL intensity in *NCD* films, which was ascribed to the presence of surface C=O bonds [144]. The results reported in [126] clearly demonstrate the applicability of the ultrathin SiV films for sensing or PL switching. The critical thickness of the diamond film within which the SiV PL can be fully switched between on and off states by oxygen and hydrogen surface terminations was estimated to 10 nm [126]. An approach to generate well spatially separated single centers, which is a prerequisite for sensing with nanoscale spatial resolution, remains to be developed.

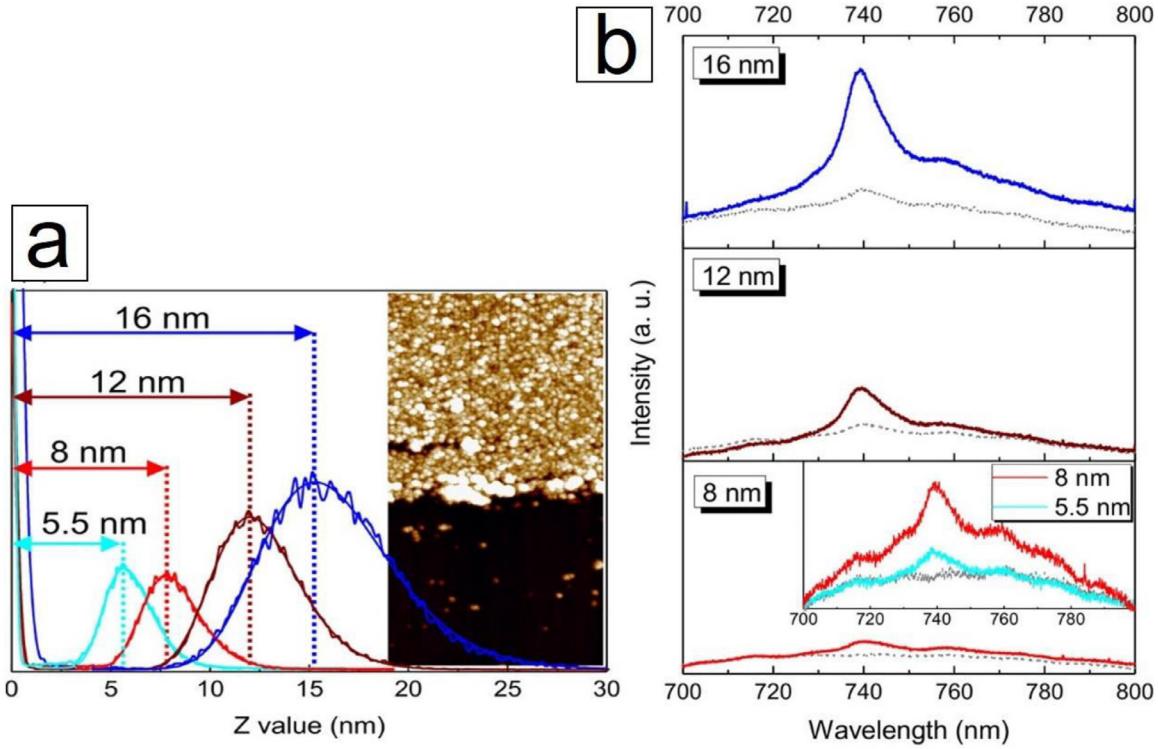

Fig. 3. (a) Histograms of atomic force microscopy (AFM) Z values of *NCD* films−Si/SiO_x substrate interfaces, showing the thickness of the *NCD* films obtained by electrostatic self-assembling seeding from 2 nm-sized diamond nanoparticles, followed by a CVD growth of the *NCD* films. Varying the potential zeta of the seed-nanodiamonds allowed varying the resulting *NCD* film thickness (from 5.5 to 16 nm). Inset: representative 1 × 0.5 μm^2 AFM top view image of the 5.5 nm-thick *NCD* film (grainy, white to brown-yellow contrast) onto the Si/SiO_x interface (Z scale is 9 nm, from dark to white). (b) Photoluminescence (PL) spectra showing the PL from the silicon-vacancy (SiV) center at 739 nm of the ultrathin Si-doped *NCD* films. The dashed grey lines correspond to the PL of as-grown *NCD* films, while the full lines (5.5 nm, cyan; 8 nm, red; 12 nm, burgundy; and 16 nm, dark blue) show an increase of the Si PL after surface oxidation. Adapted from [126] with permission. Copyright 2017, American Chemical Society.(For interpretation of the references to color in this figure legend, the reader is referred to the web version of this article.)

5. Hydrogenated graphene-based crystalline sp^3-C films

5.1. Graphane

Graphane consists of a single-layer of a hexagonal network of sp^3-bonded carbon atoms in which each carbon is bonded to one hydrogen atom, alternately above and below the layer. Its stability and formation from the hydrogenation of a single graphene sheet (1LG) were first predicted by Sofo et al. [145]. Graphane could be considered as the first member in the series of diamanes of increasing thickness as discussed below. Graphane remains elusive. Since the first experimental description of hydrogenated 1LG [146], only partially hydrogenated material has been prepared [11,14], despite it has been claimed otherwise [147]. In [147], full hydrogenation was not achieved as evidenced in the published Raman spectra which only contain sp^2-C features. The work reported in [147] claims that a small residual sp^2 phase dominates the spectra because of the much larger Raman diffusion cross-section for sp^2-C than for sp^3-C. However, in fully fluorinated graphene (wrongly denominated as "fluorographene", since "fluorographane" would be more appropriate), sp^2-C features are not observed in visible Raman spectra [148]. According to the estimation in [11], the hydrogenation rate in [147] is about 10 at.%, a value that is considered as the highest hydrogenation rate achieved by gas phase methods [11,14], which are applicable for nanoelectronics and photonics applications. The liquid phase hydrogenation methods are more efficient, as they can generate a maximum of ~76 at.% of hydrogenated carbon atoms in few-layer graphene (FLG) [149]. However, the hydrogenation of the basal planes was not evidenced in [149]. Fourier transform infrared spectroscopy (FTIR) spectra provided in [149] cannot determine whether either basal planes or only grain boundaries are hydrogenated [14]. Typical FTIR spectra reported in [149] exhibit a wide multi-component C–H stretching band including sp^3-C–H_3 and sp^3-C–H_2 modes instead of a single sp^3-C–H mode (Fig. 4), consistent with graphene domains of reduced size which are hydrogenated only on their edges by aliphatic groups [14]. The spectra from [149] in Fig. 4a are plotted between 2750 and 3000 cm^{-1}, therefore they do not include the possible contributions to the C–H band between 3100 and 3000 cm^{-1}, which include the sp^2-C–H aromatic mode.

The following factors contribute to explaining the so far unsuccessful synthesis of graphane:

(i) The lack of using suitable characterization techniques to directly evidence sp^3-C–H. As highlighted in [11,14], only few studies [149–153] reported direct quantitative data on hydrogenation rate from reliable techniques such as combustion elemental analysis or nuclear magnetic resonance. This may be due to the small amount of material processed in most cases. Furthermore, only a few studies [149–155] reported on the direct detection of C–H bonding from FTIR, which is a highly sensitive and widely accessible technique. The lack of quantitative data and FTIR analysis characterizes most of the reports on gas phase hydrogenation methods. Those studies only rely on Raman spectroscopy analysis. All studies reporting FTIR spectra failed to evidence the hydrogenation of basal planes as discussed above. To the authors' knowledge, there was no FTIR mapping data published until 2019, when diamanoids were evidenced [14].

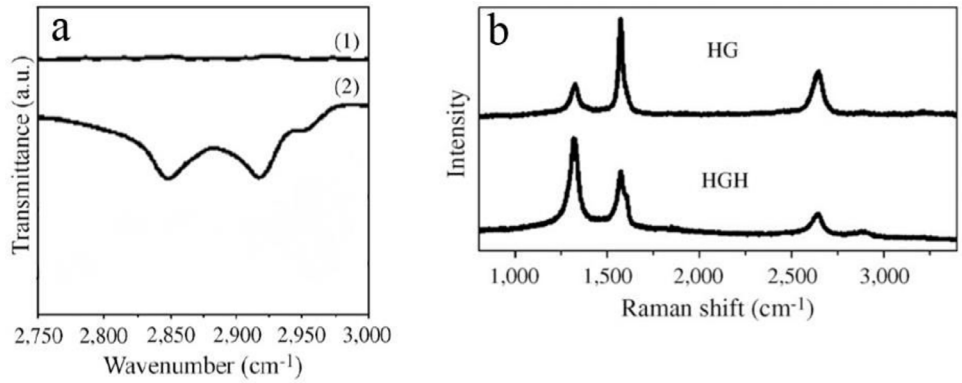

Fig. 4. (a) IR spectra of FLG prepared by the exfoliation of graphite oxide (1) before and (2) after reduction by the Birch reduction with lithium in liquid ammonia. (b) Raman spectrum of FLG prepared by the arc evaporation of graphite under hydrogen (top) before and (bottom) after reduction. Adapted from [149] with permission, Copyright 2011, National Academy of Sciences.

(ii) The misuses of Raman spectroscopy. Although Raman spectroscopy probes indiscernibly any kind of defects (*i.e.* both point or line defects, such as vacancies, edges and C–H bonding), it was used as an indirect method to detect C–H bonding in hydrogenated graphene [147]. In some of the studies, the fact that all of the defect-related peaks in Raman spectra were suppressed or highly attenuated upon annealing or laser irradiation of hydrogenated graphene materials was used to claim that defects generated during the hydrogenation treatment are C–H bonding [147]. However, Raman spectroscopy using single-point measurement cannot determine whether H is bonded to the surface of the layers or only to the edges. To the authors' knowledge, this last paramount point was not addressed in the literature before 2019. Likewise, there is no Raman mapping analysis published for hydrogenated graphene while such analysis has been widely used for graphene research. The empirical analysis of Raman D and G peak intensity ratio from an unknown number of single-point measurements was used to estimate hydrogenation rates [156]. Furthermore, Raman scattering from sp^2-C is a resonant process for visible wavelength excitation and result in a 50 to 230-fold signal enhancement relative to that of non-resonant sp^3-C Raman scattering [27]; thus, it is necessary to employ UV excitation (using low power conditions to avoid any modification of the irradiated sample) to obtain a more evenly weighted probing of both sp^3-C and sp^2-C sites. To the best of the authors' knowledge, there is no report on UV Raman spectroscopy analysis of hydrogenated graphene before 2019.

(iii) The lack of understanding of the hydrogenation mechanisms of graphene (1LG and FLG, respectively), in particular for the characterization issues raised above. There are contradictory results and interpretations concerning differences in reactivity for 1LG and FLG [146,147,157–161]. Hence, it is impossible to compare the results published so far. This is due to differences regarding the graphene materials, substrates, methods and conditions used for the hydrogenation. Also, all the reports published before 2019 [14] failed to show that hydrogen is effectively bonded to basal plane as discussed above.

It is expected that the recently successful synthesis of diamane and diamanoids thanks to the hydrogenation of FLG by H radicals, as evidenced by UV Raman mapping and FTIR microscopy (see next Section 5.2), should stimulate further research on graphane synthesis, even if graphane is significantly less stable than diamane [145]. The calculated graphane formation energy is –0.15 eV/atom according to [145] or –0.11 eV/atom according to [162] while it is of ∼–0.69–0.70 eV/atom for diamane [162].

5.2. Diamanes and diamanoids

5.2.1. Synthesis

This Section will be limited to stable genuine diamanes and diamanoids, *i.e.* only composed of carbon and hydrogen. Unstable materials obtained under pressure will not be considered as they are not practically useful. Genuine diamanes and diamanoids are new members of the 2D nanocarbon family that were recently synthesized [13–17]. Previous report on a structure transformation of FLG into a diamond-like layer failed to evidence the crystallinity of the final material [163]. Neither Raman spectra nor electron diffraction patterns were reported. The material obtained in [163] may have been sp^3-C-rich amorphous carbon [41,63]. Genuine diamane consists of two crystalline sp^3-bonded carbon layers wherein half of the carbons from both layers are hydrogenated while the other half are bonded to each other, thereby covalently bonding the layers (Fig. 5a) [162].

The material stability and formation from the hydrogenation of suspended bilayer graphene (2LG) were first predicted by Chernozatonskii et al. in 2009 [162]. Two structural configurations are possible, depending on whether the stacking sequence in the starting 2LG is AB or AA. The former will result in the diamond structure-based diamane (called diamane I in [162]), while the latter will result in the lonsdaleite structure-based diamane (called diamane II in [162]). A review on diamane was recently published [164]. Diamanoids are crystalline sp^3-bonded 2D carbon materials either similar to diamane but composed of more than two layers (Fig. 5b), or with only one outer hydrogenated layer whatever the number of layers [14,17]. A key condition for diamanoids to be formed, however, is that the starting FLG has to be of the AAA*etc.* or ABC*etc.* stacking types. Should the starting FLG be of the ABA*etc.* or turbostratic, only diamanoid/graphene hybrids may form, because the positions of the atoms are not suitable for the sp^2-C to sp^3-C conversion to propagate throughout the layers. The conversion of FLG on a metal surface into a diamanoid through the hydrogenation of the upper graphene layer is also possible. In this case, only the top surface is hydrogenated indeed, as a strong hybridization between the sp^3 dangling bond orbitals and the metallic surface orbitals is able to stabilize the bottom sp^3-bonded carbon layer without requesting actual C–H bonding [163,165].

"Diamone" was recently used to refer to one-sided hydrogenated diamane [166], possibly to follow the previous denomination of "graphone" referring to semihydrogenated graphene sheet [167]. As graphone and diamone could be understood as oxygen functionalized materials following organic chemistry nomenclature (i.e. ketones), the unambiguous denominations "one-sided hydro-

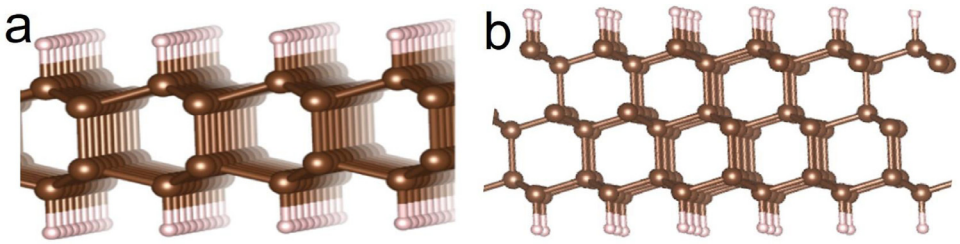

Fig. 5. Examples of (a) diamane (here diamane I) and (b) diamanoid (3 layers); brown: carbon; white: hydrogen.

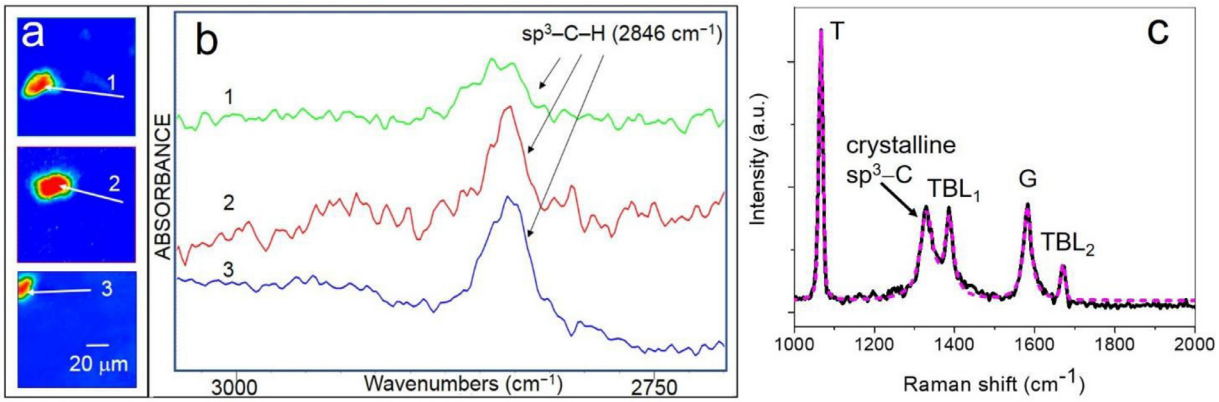

Fig. 6. (a) FTIR-ATR microscopy images processed on the integrated intensity of the associated C–C stretching band at ~1609 cm^{-1} that co-localizes with the C–H stretching band of diamanoids; (b) Typical absorbance FTIR spectra (sums of 10 to 25 spectra per spectrum) taken from pixels within the red regions arrowed in (a) [17]; (c) typical UV Raman spectrum of a diamanoid/graphene hybrid, in the case of incomplete sp^2-C to sp^3-C conversion. The spectrum shows the crystalline sp^3-C peak at 1319–1337 cm^{-1}. The T peak is generated by the interaction of a sp^3-C layer with free p_z orbitals and a graphene layer underneath. The G band reveals that the conversion of the starting FLG into a diamanoid was partial. Two peaks typical of twisted 2LG (see text), labeled TBL_1 and TBL_2, are also observed at ~1385 cm^{-1} and ~1669 cm^{-1}. An example of the fitting made by using symmetric Voigt functions (dashed line) to estimate peak positions is provided [14,17].

genated graphene" and "one-sided hydrogenated diamane" seem preferable.

The successful synthesis of stable diamanoids and diamanes was achieved by using the so-called hot-filament process. Briefly, H radicals are produced from the W-catalyzed decomposition of molecular H_2 at very high temperature (~2300 °C) while the starting graphene material (partially suspended 2LG or FLG) is maintained at low temperature (~300 °C) and low pressure (~100 Torr). H radicals chemisorb on the outer graphene basal planes on both sides, hence provoking the sp^2-C to sp^3-C conversion in those layers, and then subsequently provoking the same in the graphene layer(s) underneath, along with the interlayer bonding [14,17,163]. FTIR microscopy (Attenuated Total Reflection mode) showed that: *(i)* a single sp^3-C–H bonding type is formed; *(ii)* carbon atoms bond to only one hydrogen, and *(iii)* basal planes are fully hydrogenated, *i.e.*, not only at the edges (Fig. 6a and 6b) [14,17].

The sp^3-C stretching peak at around 1319–1337 cm^{-1} (i.e. diamond E_{2g} mode) was detected in visible and UV Raman spectra (Fig. 6c) [14–17]. Because the starting FLGs (typically 1–6 monolayers) were grown by CVD on Ni substrate, and therefore because the layers within each grain were likely to be Bernal (ABAB) stacked or rotationally faulted (turbostratic structure), the conversion was partial only [14,15,17], resulting in diamanoid/graphene hybrids [15,17]. This is the reason why the following other peaks were observed in Raman spectra (Fig. 6c): *(i)* the sharp T peak at ~1055–1071 cm^{-1}, which was shown to originate from a combination of the sp^3-C stretching mode of a sp^3-C layer with the optical out-of-plane mode of a graphene layer [15,17]; *(ii)* the G peak from graphene; and *(iii)* two sharp peaks, labelled TL_1 and TL_2, at around 1385 and 1669 cm^{-1}, respectively, which were shown to originate from twisted-bilayer graphene [15,17]. Raman mapping of the sp^3-C stretching mode peak showed diamanoid formation over extended regions of up to about 33 × 51 μm^2 [14,17]. It was supposed that the conversion took place in regions where the FLGs were Bernal-stacked [14,15,17], thus preventing the propagation of the sp^2 to sp^3 conversion beyond the first two layers.

By switching from FLG to 2LG (prepared from superposing two CVD-grown 1LGs, intrinsically poly-domains, onto each other), the hot-filament-promoted hydrogenation process was able to produce genuine diamanes from regions of the 2LG where the superimposed domains were AB- or AA-stacked [16,17], as identified using very-low-energy electron diffraction at 5 keV [16,17,35]. UV Raman mapping of the converted material revealed the only sp^3-C stretching mode peak (i.e. diamond E_{2g} mode or lonsdaleite A_{1g} and E_{2g} modes) in diamane over 20 μm-large regions, as limited by the maximum size of the coherent domains in the starting 2LG, inherent to its polycrystalline nature (Fig. 7) [16,17].

In both cases (i.e. diamane from 2LG and diamanoid/graphene hybrids from FLG), the areas of the material which appear fully or partially converted show several evidences of high stress, due to the vicinity of non-converted domains, either in the in-plane direction or perpendicular to it. In the case of diamane, those evidences are the followings:

(i) Cracks were observed in TEM images [16,17].
(ii) A 30 cm^{-1} wavenumber shift of the sp^3-C stretching Raman peak was observed, which was interpreted as revealing a stress of up to about 10 GPa [16,17].
(iii) Evidences of significant local distortions calculated by first principle calculations on modified diamane structures (i.e. underhydrogenated structure, achieved by removing 7 H atoms from the top layer of genuine diamane structure) [16,17].

In the case of diamanoid/graphene hybrids, high stress was revealed by the following results:

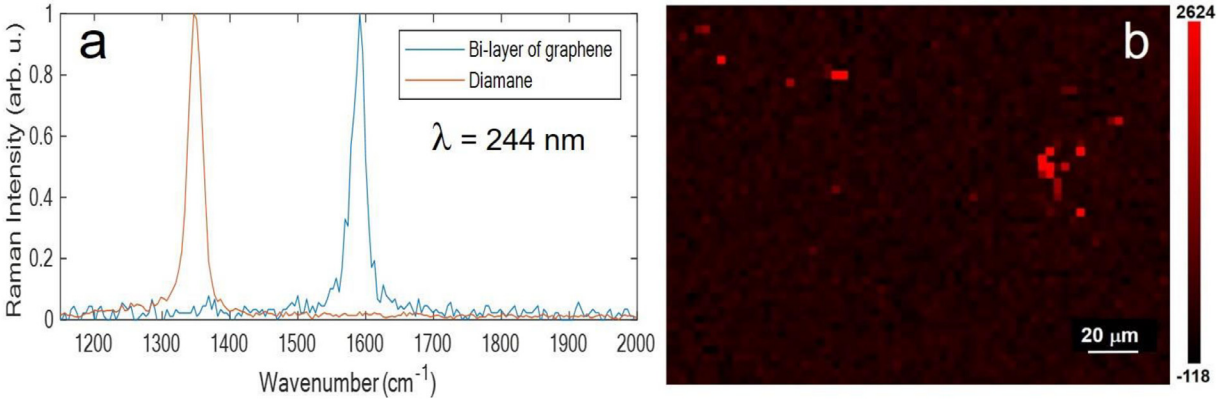

Fig. 7. (a) Typical Raman spectrum (taken at 244 nm) of the starting 2LG (blue) superimposed with that of the resulting diamane (red) after hydrogenation; (b) example of intensity map of the sp^3-C stretching mode after hydrogenation of the 2LG [16,17].(For interpretation of the references to color in this figure legend, the reader is referred to the web version of this article.)

(i) The formation of twisted bilayer graphene as evidenced by electron diffraction and Raman spectroscopy [15,17]. It was supposed that the slight rotation of graphene sheets was induced by the relaxation of huge (several GPa) local constraints that developed between superimposed layers as a result of the sp^2-C-to-sp^3-C conversion [15,17].

(ii) A downshift by almost 150 cm^{-1} of the G peak calculated by Density Functional Theory from a model of partially hydrogenated and converted systems consisting of four distinct carbon layers, revealing a stress of about 33 GPa, which is by far enough to generate the delamination and twisting events that were experimentally observed in the material [15,17].

Generally speaking, the hot-filament process was successful in synthesizing diamanoid/graphene hybrids and diamane for the following reasons: *(i)* it is very efficient to produce atomic hydrogen (H); *(ii)* H recombination reactions are sufficiently slow at the typical process pressures (below 100 Torr) for H to be present at super-equilibrium concentration throughout most of the reactor volume [168]; *(iii)* as compared to low-pressure plasma techniques, the presence of ions accelerated toward the substrate, which can etch the graphene film [156], is avoided; *(iv)* low substrate-temperature conditions can be used. Such conditions were previously used to conformally coat carbon nanotube bundles with diamond nanocrystals before the nanotubes could be etched away [17,169,170].

It is believed that diamane dimensions are only limited by the dimensions of the coherently stacked domains in the starting polydomain graphene, not by the process. The key for producing homogenous diamane films now only relies on starting from a good quality 2LG material, that is to say, ideally, single-crystal AB flakes as large as possible.

5.2.2. Potential applications

According to calculations, diamanes and diamanoids are semiconducting materials, with a direct wide band-gap (> 3 eV in the case of diamane) which depends on the stacking order and number of layers [162,171,172], which is very attractive for nanoelectronics, band-gap engineering and active laser medium in nanooptics. Because of its expected high thermal conductivity, diamanes and diamanoids may be used in thermal management devices [173]. For diamane, calculations have predicted a room thermal conductivity higher than 2034 W/m.K and a ballistic thermal conductance of 2.95 $GW/m^2.K$ [174]. Owing to the lower effective Bohr radius of defects and higher radiative electronic transition rate, calculations have shown that diamane is a better host system for single photon emission than diamond [175]. Diamanes and diamanoids are expected to be mechanically very strong; therefore, they may be very attractive for ultrathin protective coatings, ultrahigh-strength components in composite materials for aerospace applications for instance, and nano-electromechanical systems [173]. Because of the expected low friction coefficient of the hydrogenated surface, diamanoids may be used to improve the wear resistance of coated mechanical parts [14]. The expected strength, low coefficient of friction and bio-compatibility could render diamanes and diamanoids very competitive as building materials to make lower power and miniaturized electronics and implantable biomedical devices [14]. A diamane nanoribbon resonator was calculated to possess a high natural frequency, high quality factor, high figure of merit, high in-plane stiffness and, as opposed to graphene, to be free from the influence of the edge configuration; consequently, it would be better than 1LG, 2LG, MoS_2, or other 2D material resonators (at least for the 1–300 K temperature range) [176]. Hetero-structures of graphene and diamane, in other words diamanoid/graphene hybrids, would be attractive for tunnel devices, optical linear waveguides, high efficiency optoelectronic sensors, lithium batteries, and supercapacitors [162,173]. As detailed above (Section 3.3.1), amorphous carbon films face significant challenges to meet the demand of hard drive industry to enable HAMR technology. As a substitute, sub-2 nm thick diamanoid could be of great interest if they can withstand high recording temperature, above 500 °C. As detailed above (Section 3.3.2), amorphous carbon could be very promising low-k dielectric materials to improve the performance of nano-electronic metal interconnect structures. However, their poor thermal conductivity is too prohibitive, hence diamanes and diamanoids may constitute better candidates for this, even if they may show anisotropic properties. Overall, the valuable benefits which come with this new family of materials are as follows:

(i) They are wide band-gap semiconducting materials as mentioned above.

(ii) They are expected to have a lower k-constant than bulk diamond (k = 5.7); presumably similar to that of *a-C:H* (in the range 2.6–3.3).

(iii) They are expected to exhibit low leakage-current and high breakdown-voltage considering diamond properties (diamond breakdown-voltage is 10 MV/cm [105], hence higher than that of *a-C:H* as previously indicated (~8 MV/cm).

(iv) Their room-temperature in-plane thermal conductivity (calculated to be higher than 2034 W/m.K [174]) and ballistic thermal conductance (calculated to be of 2.95 $GW/m^2.K$ [174]) are significantly higher than for many 2D and 3D materials, including *NCD* and *UNCD* [177]. High transverse thermal conductivity may

be possible. Their coefficient of thermal expansion is expected to be low considering diamond properties [105].

(v) They are expected to exhibit high strength, hardness, Young modulus, fracture toughness, comparable to that of diamond [178] or lonsdaleite [179]. They are expected to have high in-plane stiffness (calculated to be 715 N/m in the case of diamane) [162]. They are expected to have low bending stiffness (large bending flexibility) considering the calculated properties of some diamond nanothreads [180], which would be of great interest for flexible electronics.

(vi) Specific to one-sided hydrogenated diamanoids, they are expected to show high adhesion strength because of the strong hybridization between the diamanoid sp^3 dangling bond orbitals and the metallic surface orbitals [163,165].

(vii) They are produced by a technology used for more than 40 years for diamond coating production [181,182].

(viii) They are much easier to process as nanoscale layers and structures than diamond [105].

(ix) They are expected to offer good resistance to Cu diffusion considering previous results on *a-C:H* [108] and the very low solubility of C in Cu (~0.008 weight % at ~1084 °C) [183].

(x) They are expected to offer high chemical inertness considering that of diamond and *a-C:H* [41]. In particular, they are expected to offer good chemical resistance to ambient H_2O/O_2 together with wet chemical diffusion considering the behavior of *a-C:H* used as gas-impermeable coating onto the inside wall of polyethylene bottles to improve the packaging for a variety of drinks, where the permeation of CO_2, H_2O, and O_2 needs to be suppressed [50,184], or considering the performance of sub-2 nm amorphous carbon films used as corrosion barrier and wear resistant coating of hard disk drives [50,84] and optical storage systems such as CDs and DVDs [86,87].

(xi) They will not be a source of amines that would trigger resist poisoning [103]. This is a strong advantage over amorphous-BN and BN layers, which could be considered as the main 2D material competitors [185].

Therefore, generally speaking, diamanes and diamanoids exhibit better properties than that of all types of sp3C2D, or equivalent for the least, with the benefit of an easy and up-scalable processability.

6. Conclusion

In the past four years, the field of nanometer-thick sp^3-bonded-carbon-rich films (sp3C2D) has experienced various significant breakthroughs, which include the synthesis of sub-10 nm nanocrystalline diamond (*NCD*), monolayer amorphous carbon (*MAC*), and genuine diamanes and diamanoids. Those advances have completed the older achievements obtained in the field of sub-10 nm tetrahedral amorphous carbon films, which have been used in hard drive technology for many years and which have been explored as a promising low-k dielectric material for VLSI. Those breakthroughs could stimulate the synthesis of additional new sp3C2D such as graphane and a variety of *MACs* including some in which sp^3-C would prevail over sp^2-C. sp3C2D films share exceptional combination of chemical and physical properties that is of particular interest for the development of a wide range of applications. They can be produced by PVD or CVD techniques compliant with the semiconductor industry. Because they are based on two of the most abundant elements on Earth (carbon, hydrogen), and because the capture of the excess gaseous forms of carbon into those materials could enable a double-winning strategy, they are compatible with sustainable development. They could compete in various key applications where they could offer strong advantages over graphene or other materials, such as transition metal dichalcogenides, which are more challenging to manufacture and integrate, exhibit higher mass density, and include chemical elements the natural availability of which might be questionable at more or less short term. Key potential applications include host-materials for single photon emission, structural materials for nano-electromechanical devices (diamanoids, diamane, *NCD*), low-*k* dielectric materials with super-high thermal conductivity for interconnects, wide-band-gap materials for transistors (diamanoids), protecting coating for hard drive technology (*NCD*, diamanoids) and resonators (diamane). The interest in amorphous carbon in some applications may fall to the benefit of diamanoids if the latter can exhibit appropriate thermal stability.

The synthesis of those new sp^3-bonded carbon nanomaterials should motivate further work, such as:

(i) The improvement of the synthesis methods, for instance to obtain graphenes with large area single coherent domains as a better source material for diamanes and diamanoids, or to further reduce the thickness of pinhole-free *NCD*.

(ii) The research on new synthesis routes such as the direct synthesis of diamane and diamanoid from hydrocarbon precursors.

(iii) The study of physical properties and the development of new devices for a wide range of applications;

(iv) The study of thermal stability of diamanes and diamanoids.

(v) The resumption of the quest for graphane and the search for new nanomaterials such as a whole family of monolayer amorphous carbon films beyond *MAC, i.e.*, including an increasing contribution of sp^3-C.

(vi) The study of the potential interest of diamanoid/graphene hybrids, and more generally of sp^3-bonded carbon nanofilm/graphene combinations for carbon-based electronics.

Declaration of interests

The authors declare that they have no known competing financial interests or personal relationships that could have appeared to influence the work reported in this paper.

Data Availability

Data will be made available on request.

Acknowledgments

This research was funded by the Ministry of Higher Education, Science and Technology of the Dominican Republic (2018-2019 (No. 2018-2019-1A2-087) and 2020-2021 (No. 2020-2021-1A1-066) FONDOCyT programs). The research also received support from CNRS (France) through the French-Dominican International Research Project NEWCA.

References

[1] K.S. Novoselov, A.K. Geim, S.V. Morozov, D. Jiang, Y. Zhang, S.V. Dubonos, I.V. Grigorieva, A.A. Firsov, Electric field effect in atomically thin carbon films, Science 306 (2004) 666–669.

[2] A.C. Ferrari, F. Bonaccorso, V. Fal'ko, K.S. Novoselov, S. Roche, P. Bøggild, et al., Science and technology roadmap for graphene, related two-dimensional crystals, and hybrid systems, Nanoscale 7 (2015) 4598–4810.

[3] N. Briggs, S. Subramanian, Z. Lin, X.; Li, X. Zhang, K. Zhang, K. Xiao, D. Geohegan, R. Wallace, L.-Q. Chen, M. Terrones, A. Ebrahimi, S. Das, J. Redwing, C. Hinkle, K. Momeni, A. van Duin, V. Crespi, S. Kar, J.A. Robinson, A roadmap for electronic grade 2D materials, 2D Mater. 6 (2) (2019) 022001.

[4] A. Castellanos-Gomez, Black phosphorus: narrow gap, wide applications, J. Phys. Chem. Lett. 6 (2015) 4280–4291.

[5] H. Oughaddou, H. Enriquez, M.R. Tchalala, H. Yildirim, A.J. Mayne, A. Bendounane, G. Dujardin, M.A. Ali, A. Kara, Silicene, a promising new 2D material, Progr. Sur. Sci. 90 (1) (2015) 46–83.

[6] J.-H. Park, J.C. Park, S.J. Yun, H. Kim, D.H. Luong, S.M. Kim, S.H. Choi, W. Yang, J. Kong, K.K. Kim, Y.H. Lee, Large-area monolayer hexagonal boron nitride on Pt foil, ACS Nano 8 (2014) 8520–8528.

[7] P.V. Bakharev, M. Huang, M. Saxena, S.W. Lee, S.H. Joo, S.O. Park, J. Dong, et al., Chemically induced transformation of chemical vapour deposition grown bilayer graphene into fluorinated single-layer diamond, Nat. Nanotechnol. 15 (2020) 59–66.

[8] S. Manzeli, D. Ovchinnikov, D. Pasquier, O.V. Yazyev, A. Kis, 2D transition metal dichalcogenides, Nat. Rev. Mater. 2 (8) (2017) 1–15.

[9] S. Venkateshalu, A.N. Grace, MXenes—a new class of 2D layered materials: synthesis, properties, applications as supercapacitor electrode and beyond, Appl. Mater. Today 18 (2020) 100509.

[10] F. Piazza, M. Monthioux, Ultra-thin carbon films: the rise of sp3-C-based 2D materials?, C 7, 30 (2021).

[11] M Pumera, CHA. Wong, Graphane and hydrogenated graphene, Chem. Soc. Rev. 42 (2013) 5987–5995.

[12] A. Bianco, Y. Chen, Y. Chen, G. Debjit, R.H. Hurt, Y.A. Kim, N. Koratkarhi, V. Meunier, M. Terrones, A carbon science perspective in 2018: current achievements and future challenges, Carbon 132 (2018) 785–801.

[13] F. Piazza, Sp3-bonded carbon materials, methods of manufacturing and uses thereof. WO Patent 2019 233901, 5 June 2018.

[14] F. Piazza, K. Gough, M. Monthioux, P. Puech, I. Gerber, R. Wiens, G. Paredes, C. Ozoria, Low temperature, pressureless sp^2 to sp^3 transformation of ultra-thin, crystalline carbon films, Carbon 145 (2019) 10–22.

[15] F. Piazza, M. Monthioux, P. Puech, I. Gerber, Towards a better understanding of the structure of diamanoïds and diamanoïd/graphene hybrids, Carbon 156 (2020) 234–241.

[16] F. Piazza, P. Puech, I. Gerber, K. Cruz, M. Monthioux, Raman evidence for the successful synthesis of diamane, Carbon 169 (2020) 129–133.

[17] Piazza F.; Monthioux M.; Puech P.; Gerber I.C.; Gough K. Progress on diamane and diamanoid thin film pressureless synthesis, C 7(1), 9 (2021).

[18] P.K. Chu, L. Li, Characterization of amorphous and nanocrystalline carbon films, Mater. Chem. Phys. 96 (2006) 253.

[19] P. van der Heide, X-Ray Photoelectron Spectroscopy: An Introduction to Principles and Practices, John Wiley & Sons, Inc, 2012.

[20] F.J. Himpsel, F.R. McFeely, A. Taleb-Ibrahimi, J.A. Yarmoff, G. Hollinger, Microscopic structure of the SiO_2/Si interface, Phys. Rev. B 38 (1988) 6084.

[21] J. Diaz, G. Paolicelli, S. Ferrer, F. Comin, Separation of the sp^3 and sp^2 components in the C 1s photoemission spectra of amorphous carbon films, Phys. Rev. B 54 (1996) 8064–8069.

[22] S. Turgeon, R.W. Paynter, On the determination of carbon sp^2/sp^3 ratios in polystyrene-polyethylene copolymers by photoelectron spectroscopy, Thin. Solid Films 394 (2001) 44–48.

[23] A.C. Ferrari, J. Robertson, Raman spectroscopy of amorphous, nanostructures, diamond-like carbon, and nanodiamond, Phil. Trans. R. Soc. Lond. A 362 (2004) 2477–2512.

[24] A. Eckmann, A. Felten, A. Mischchenko, L. Britnell, R. Krupke, K.S. Novoselov, C. Casiraghi, Probing the nature of defects in graphene by Raman spectroscopy, Nano Lett. 12 (2012) 3925–3930.

[25] E. Picheau, A. Impellizzeri, D. Rybkovskiy, M. Bayle, J.-Y. Mevellec, F. Hof, et al., Intense Raman D band without disorder in flattened carbon nanotubes, ACS Nano 15 (2021) 596–603.

[26] G. Paredes, R. Wang, P. Puech, G. Seine, J.-M. Leyssale, R. Arenal, et al., Texture, nanotexture, and structure of carbon nanotube-supported carbon cones, ACS Nano 16 (2022) 9287–9296.

[27] J. Wagner, C. Wild, P. Koidl, Resonance effects in Raman scattering from polycrystalline diamond films, Appl. Phys. Lett. 59 (7) (1991) 779–781.

[28] C. Casiraghi, F. Piazza, A.C. Ferrari, D. Grambole, J. Robertson, Bonding in hydrogenated diamond-like carbon by Raman spectroscopy, Diamond Relat. Mater. 14 (2005) 1098–1102.

[29] J. Ristein, R.T. Stief, L. Ley, A comparative analysis of a-C:H by infrared spectroscopy and mass selected thermal effusion, J. Appl. Phys. 84 (1998) 3836.

[30] J.G. Buijnsters, R. Gago, I. Jiménez, M. Camero, F. Agulló-Rueda, C. Gómez-Aleixandre, Hydrogen quantification in hydrogenated amorphous carbon films by infrared, Raman, and x-ray absorption near edge spectroscopies, J. Appl. Phys. 105 (9) (2009) 093510.

[31] J.J. Fox, A.E. Martin, Investigations of infra-red spectra. Determination of C-H frequencies (∼3000 cm-1) in paraffins and olefins, with some observations on “polythenes, Proc. R. Soc. Lond. Ser. A 175 (1940) 208–233.

[32] D.B. Williams, C.B. Carter, Transmission Electron Microscopy, A Textbook for Materials Science, Springer, 2009.

[33] B.E. Smith, D.E. Luzzi, Electron irradiation effects in single wall carbon nanotubes, J. Appl. Phys. 90 (2001) 35.

[34] K. Kanaya, K. Adachi, K. Yonehara, Y. Muranaka, H. Ishikawa, Quantitative analysis of knock-on and thermal damage of biological specimens by electron irradiation in transmission electron microscopy, Micron Microsc. Acta 22 (3) (1991) 223–237.

[35] P. Puech, I.C. Gerber, F. Piazza, M. Monthioux, Combining low and high electron energy diffractions as a powerful tool for studying 2D materials, Appl. Phys. A 127 (2021) 485.

[36] S. Waidmann, M. Knupfer, J. Fink, B. Kleinsorge, J. Robertson, Electronic structure studies of undoped and nitrogen-doped tetrahedral amorphous carbon using high-resolution electron energy-loss spectroscopy, J. Appl. Phys. 89 (2001) 3783.

[37] S.D. Berger, D.R. McKenzie, P.J. Martin, EELS analysis of vacuum arc-deposited diamond-like films, Phil. Mag. Lett. 57 (1988) 285–290.

[38] J. Kakinoki, K. Katada, T Hanawa, T. Ino, Electron diffraction study of evaporated carbon films, Acta Cryst. 13 (1960) 171–179.

[39] J. Kakinoki, K. Katada, T. Hanawa, Heat treatment of evaporated carbon films, Acta Cryst. 13 (1960) 448–449.

[40] S. Aisenberg, R. Chabot, Ion-beam deposition of thin films of diamond-like carbon, J. Appl. Phys. 42 (1971) 2953.

[41] J. Robertson, Diamond-like amorphous carbon, Mater. Sci. Eng. R 37 (2002) 129–281.

[42] W. Jacob, W. Möller, On the structure of thin hydrocarbon films, Appl. Phys. Lett. 63 (1993) 1771.

[43] M. Weiler, S. Sattel, K. Jung, H. Ehrhardt, V.S. Veerasamy, J. Robertson, Highly tetrahedral, diamond-like amorphous hydrogenated carbon prepared from a plasma beam source, Appl. Phys. Lett. 64 (1994) 2797.

[44] D.R. McKenzie, Tetrahedral bonding in amorphous carbon, Rep. Prog. Phys. 59 (1996) 1611.

[45] X. Xiao, J. Birell, J.E. Jerbi, O. Auciello, J.A. Carlisle, Low temperature growth of ultrananocrystalline diamond, J. Appl. Phys. 96 (2004) 2232.

[46] F. Piazza, J.A. González, R. Velásquez, J. De Jesús, S.A. Rosario, G. Morell, Diamond film synthesis at low temperature, Diamond Relat. Mater. 15 (2006) 109.

[47] F Piazza, G Morell, Synthesis of diamond at sub 300 °C substrate temperature, Diamond Relat. Mater. 16 (11) (2007) 1950–1957.

[48] F Piazza, F Solá, O Resto, LF Fonseca, G Morell, Synthesis of diamond nanocrystals on polyimide film, Diamond Relat. Mater 18 (2009) 113–116.

[49] K. Tsugawa, M. Ishihara, J. Kim, Y. Koga, M. Hasegawa, Nanocrystalline diamond film growth on plastic substrates at temperatures below 100°C from low-temperature plasma, Phys. Rev. B 82 (2010) 125460.

[50] C. Casiraghi, A.C. Ferrari, J. Robertson, Diamond-like carbon for data and beer storage, Materialstoday 10 (2007) 44.

[51] A. Oberlin, Carbonization and graphitation, Carbon 22 (1984) 521–541.

[52] R.C. Haddon, The fullerenes: powerful carbon-based electron acceptors, Phil. Trans. R. Soc. Lond. A 343 (1993) 53–62.

[53] A. Bianco, H.-M. Cheng, T. Enoki, Y. Gogotsi, R.H. Hurt, N. Koratkar, T. Kyotani, M. Monthioux, C.-R. Park, J.M.D. Tascon, J. Zhang, All in the graphene family – A recommended nomenclature for two-dimensional carbon materials, Carbon 65 (2013) 1–6.

[54] CT Toh, H; Zhang, J Lin, AS; Mayorov, YP Wang, CM; Ferry Orofeo, H DB; Andersen, N Kakenov, Z Guo, IH Abidi, H Sims, K Suenaga, ST Pantelides, B Özyilmaz, Synthesis and properties of free-standing monolayer amorphous carbon, Nature 577 (2020) 199–203.

[55] M.P. Siegal, J.C. Barbour, P.N. Provencio, D.R. Tallant, T.A. Friedmann, Amorphous-tetrahedral diamondlike carbon layered structures resulting from film growth energetics, Appl. Phys. Lett. 73 (1998) 759.

[56] M.P. Siegal, P.N. Provencio, D.R. Tallant, R.L. Simpson, B. Kleinsorge, W.I. Milne, Bonding topologies in diamondlike amorphous carbon films, Appl. Phys. Lett. 76 (2000) 2047.

[57] J. Matlak, K. Komvopoulos, Ultrathin amorphous carbon films synthesized by filtered cathodic vacuum arc used as protective overcoats of heat-assisted magnetic recording heads, Sci. Rep. 8 (2018) 9647.

[58] Y-H Kang, S. Lee, Y. Choi, W.K. Seong, K.H. Han, J.H. Kim, H-M. Kim, S. Hong, S.H. Lee, R.S. Ruoff, K-B Kim, S.O. Kim, Large-area uniform 1-nm-level amorphous carbon layers from 3D conformal polymer brushes. A “next-generation” Cu diffusion barrier? Adv. Mater. 34 (2022) 2110454.

[59] Y. Lifshitz, S.R. Kasi, J.W. Rabelais, Subplantation model for film growth from hyperthermal species: application to diamond, Phys. Rev. Lett. 62 (1989) 1290.

[60] Y. Lifshitz, S.R. Kasi, J.W. Rabelais, W. Eckstein, Subplantation model for film growth from hyperthermal species, Phys. Rev. B 41 (1990) 10468.

[61] Y. Lifshitz, G.D. Lempert, E. Grossman, Substantiation of subplantation model for diamondlike film growth by atomic force microscopyPhys, Rev. Lett. 72 (1994) 2753.

[62] M.A. Caro, V.L. Deringer, J. Koskinen, T. Laurila, G. Csányi, Growth mechanism and origin of high sp^3 content in tetrahedral amorphous carbon, Phys. Rev. Lett. 120 (2018) 166101.

[63] F. Piazza, Hard-hydrogenated tetrahedral amorphous carbon films by distributed electron cyclotron resonance plasma, Int. J. Refract. Met. Hard Mater. 24 (2006) 39–48.

[64] F Piazza, O Resto, G Morell, Nonlinear effects in collision cascades and high energy shock waves during ta-C: H growth, J. Appl. Phys. 102 (2007) 013301.

[65] J. Ishikawa, Y. Takeiri, k. Ogawa, T. Takagi, Preparation and structure of carbon film deposited by a mass-separated C^+ ion beam, J. Appl. Phys. 55 (1987) 188–193.

[66] D.R. McKenzie, D. Muller, B.A. Pailthorpe, Compressive-stress-induced formation of thin-film tetrahedral amorphous carbon, Phys. Rev. Lett. 67 (1991) 773–776.

[67] R. Lossy, D.L. Pappas, P.A. Roy, J.J. Cuomo, V.M. Sura, Filtered arc deposition of amorphous diamond, Appl. Phys. Lett. 61 (1992) 171–173.

[68] P.J. Fallon, V.S. Veerasamy, C.A. Davis, J. Robertson, G. Amaratunga, W.I. Milne, J. Koskinen, Properties of filtered-ion-beam-deposited diamondlike carbon as a function of ion energy, Phys. Rev. B 48 (1993) 4777–4782.

[69] D.L. Pappas, K.L. Saenger, J. Bruley, W. Krakow, J.J. Cuomo, T. Gu, R.W. Collins, Pulsed laser deposition of diamond-like carbon films, J. Appl. Phys. 71 (1992) 5675–5684.

[70] F. Xiong, Y.Y. Chang, R.P.H. Chang, Complex dielectric function of amorphous diamond films deposited by pulsed-excimer-laser ablation of graphite, Phys. Rev. B 48 (1993) 8016–8023.

[71] M. Chhowalla, C.A. Davis, M. Weiler, B. Kleinsorge, G.A.J. Amaratunga, Stationary carbon cathodic arc: plasma and film characterization, J. Appl. Phys. 79 (1996) 2237.

[72] M. Weiler, S. Sattel, T. Giessen, K. Jung, H. Ehrhardt, V.S. Veerasamy, J. Robertson, Preparation and properties of highly tetrahedral hydrogenated amorphous carbon, Phys. Rev. B 53 (1996) 1594–1608.
[73] M. Weiler, K. Lang, E. Li, J. Robertson, Deposition of tetrahedral hydrogenated amorphous carbon using a novel electron cyclotron wave resonance reactor, Appl. Phys. Lett. 72 (1998) 1314–1316.
[74] N.A. Morrison, S. Muhl, S.E. Rodil, A.C. Ferrari, M. Nesladek, W.I. Milne, J. Robertson, The preparation, characterization and tribological properties of TA-C: H deposited using an electron cyclotron wave resonance plasma beam source, Phys. Stat. Sol. (a) 172 (1999) 79–90.
[75] F. Piazza, G. Morell, Wettability of hydrogenated tetrahedral amorphous carbon, Diamond Relat. Mater. 18 (2009) 43–50.
[76] F. Piazza, D. Grambole, F. Herrmann, G. Relihan, M.F. Barthe, P. Desgardin, et al., Incorporation of hydrogen and oxygen into (t)a-C: H thin films deposited using DECR plasma, Mater. Res. Soc. Proc. 675 (2001).
[77] A.C. Ferrari, A. Libassi, B.K. Tanner, V. Stolojan, J. Yuan, L.M. Brown, S.E. Rodil, B. Kleinsorge, J. Robertson, Density, sp^3 fraction, and cross-sectional structure of amorphous carbon films determined by x-ray reflectivity and electron energy-loss spectroscopy, Phys. Rev. B 62 (2000) 11089–11103.
[78] A.C. Ferrari, J. Robertson, M.G. Beghi, C.E. Bottani, R. Ferulano, R. Pastorelli, Elastic constants of tetrahedral amorphous carbon films by surface Brillouin scattering, Appl. Phys. Lett. 75 (1999) 1893–1895.
[79] P. Koidl, C. Wild, B. Dischler, J. Wagner, M. Ramsteiner, Properties and characterization of amorphous carbon films, Mater. Sci. Forum 52 (1990) 41.
[80] M.A. Tamor, W.C. Vassell, K.R. Carduner, Atomic constraint in hydrogenated "diamond-like" carbon, Appl. Phys. Lett. 58 (1991) 592–595.
[81] J.W. Zhou, K.S. K.Reichelt, B. Dischler, The deposition and study of hard carbon films, J. Appl. Phys. 65 (1989) 3914–3918.
[82] W. Möller, Plasma and surface modelling of the deposition of hydrogenated carbon-films from low pressure methane plasmas, Appl. Phys. A-Mater. 56 (1993) 527–546.
[83] K.B.K. Teo, S.E. Rodil, J.T.H. Tsai, A.C. Ferrari, J. Robertson, W.I. Milne, Effect of graphitic inclusions on the optical gap of tetrahedral amorphous carbon films, J. Appl. Phys. 89 (2001) 3706.
[84] A.C. Ferrari, Diamond-like carbon for magnetic storage disks, Surf. Coat. Technol. 180-181 (2004) 190–206.
[85] C. Morsbach, C. Dubarry, M. Gabriel, M. Hoyer, S. Knappmann, F. Piazza, et al., Flyable media for slider based ultra-high density optical recording, IEE Proc.-Sci., Meas. Technol. 150 (5) (2003) 203–206.
[86] F. Piazza, D. Grambole, L. Zhou, F. Talke, C. Casiraghi, A.C. Ferrari, J. Robertson, Large area deposition of hydrogenated amorphous carbon films for optical storage disks, Diamond Relat. Mater. 13 (2004) 1505–1510.
[87] F. Piazza, D. Grambole, D. Schneider, C. Casiraghi, A.C. Ferrari, J. Robertson, Protective diamond-like carbon coatings for future optical storage disks, Diamond Relat. Mater. 14 (2005) 994.
[88] P.R. Goglia, J. Berkowitz, J. Hoehn, A. Xidis, L. Stover, Diamond-like carbon applications in high density hard disc recording heads, Diamond Relat. Mater. 10 (2001) 271–277.
[89] V. Novotny, N. Staud, Correlation between environmental and electrochemical corrosion of thin film magnetic recording media, J. Electrochem. Soc. 135 (1998) 2931–2938.
[90] J. Gui, Tribology challenges for head-disk interface toward 1 Tb/in^2, IEEE Trans. Magn. 39 (2003) 716–721.
[91] B. Marchon, N. Heiman, M.R. Khan, Evidence for tribological wear on amorphous carbon thin films, IEEE Trans. Magn. 26 (1990) 168–170.
[92] N.H. Cho, K.M. Krishnan, D.K. Veirs, M.D. Rubin, C.B. Hopper, B. Bhushan, Chemical structure and physical properties of diamond-like amorphous carbon films prepared by magnetron sputtering, J. Mater. Res. 5 (1990) 2543–2554.
[93] P.B. Leezenberg, W.H. Johnston, G.W. Tyndall, Chemical modification of sputtered amorphous-carbon surfaces, J. Appl. Phys. 89 (2001) 3498.
[94] N. Wang, K. Komvopoulos, F. Rose, B. Marchon, Structural stability of hydrogeanted amorphous carbon overcoats used in heat-assisted magnetic recording investigated by rapid thermal annealing, J. Appl. Phys. 113 (2013) 083517.
[95] B.K. Pathem, X.-C. Guo, F. Rose, N. Wang, K. Komvopoulos, E. Schreck, B. Marchon, Carbon overcoat oxidation in heat-assisted magnetic recording, IEEE Trans. Mag. 49 (2013) 3721–3724.
[96] B. Marchon, T. Pitchford, Y-T. Hsia, S. Gangopadhyay, The head-disk interface roadmap to an areal density of 4 Tbit/in^2, Adv. Tribol. 2013 (2013) 521086.
[97] N. Dwivedi, E. Rismani-Yazdi, R.J. Yeo, P.S. Goohpattader, N. Satyanarayana, N. Srinivasan, B. Druz, S. Tripathy, C.S. Bhatia, Probing the role of an atomically thin SiN_x interlayer on the structure of ultrathin carbon films, Sci. Rep. 4 (2014) 5021.
[98] R. Ji, Y. Ma, M. Shakerzadeh, H.L. Seet, J.F. Hu, Laser irradiation effect on carbon overcoat for HAMR application, Surf. Interface Anal. 46 (2014) 204–208.
[99] N. Dwivedi, A.K. Ott, K. Sasikumar, C. Dou, R.J. Yeo, B. Narayanan, U. Sassi, D. De Fazio, G. Soavi, T. Dutta, O. Balci, S. Shinde, J. Zhang, A.K. Katiyar, P.S. Keatley, A.K. Srivastava, S.K.R.S. Sankaranarayanan, A.C. Ferrari, C.S. Bhatia, Graphene overcoats for ultra-high storage density magnetic media, Nat. Commun. 12 (2021) 2854.
[100] G. Moore, Cramming more components onto integrated circuits, Proc. IEEE 86 (1) (1998) 82.
[101] S.H. Brongersma, M. Blauw, M. Zevenbergen, D. Karabacak, R. Vitushinsky, M.C.C. Van Ann Dam, R. Vullers, Z. Zeng, R. van Schaijk, More moore meets more than moore: enabling healthcare applications, Phys. Stat. Sol. C 11 (2014) 46.
[102] G. Zhang, A. van Roosmalen, More than Moore: Creating High Value Micro/Nanoelectronics Systems, Springer, New York, 2009.
[103] S.W. King, Dielectric barrier, etch stop, and metal capping materials for state of the art and beyond metal interconnects, ECS J. Solid State Sci. Technol. 4 (2015) N3029–N3047.
[104] M. Jenkins, D.Z. Austin, J.F. Conley Jr., J. Fan, C.H. de Grott, L. Jiang, Y. Fan, R. Ali, G. Ghosh, M. Orlowski, S.W. King, Review-Beyond the heights and lows: a perspective on the future of dielectrics research for nanoelectronics devices, ECS J. Solid State Sci. Technol. 8 (11) (2019) N159–N185.
[105] C.J.H. Wort, R.S. Balmer, Diamond as an electronic material, Mater. Today 11 (1-2) (2008) 22–28.
[106] J.C. Phillips, Dielectric Definition of Electronegativity, Phys. Rev. Lett. 20 (1968) 550.
[107] A. Grill, Amorphous carbon based materials as the interconnect dielectric in ULSI, Diamond Relat. Mater. 10 (2001) 234–239.
[108] K.S. Kim, Y.C. Jang, H.J. Kim, Y.-C. Quan, J. Choi, D. Jung, N.-E. Lee, The interface formation and adhesion of metals (Cu, Ta, and Ti) and low dielectric constant polymer-like organic thin films deposited by plasma-enhanced chemical vapor deposition using para-xylene precursor, Thin Solid Films 377-378 (2000) 122–128.
[109] S. Takabayashi, M. Yang, S. Ogawa, H. Hayashi, R. Ješko, T. Otsuji, Y. Takakuwa, Relationship between the structure and electrical characteristics of diamond–like carbon films, J. Appl. Phys. 116 (2014) 093507.
[110] M. Shamsa, W.L. Liu, A.A. Balandin, C. Casiraghi, W.I. Milne, A.C. Ferrari, Thermal conductivity of diamond-like carbon films, Appl. Phys. Lett. 89 (2006) 161921.
[111] J.E Butler, A.V. Sumant, The CVD of Nanodiamond Materials, Chem. Vap. Dep. 14 (2008) 145–160.
[112] D.M. Gruen, X.Z. Pan, A.R. Krauss, S.Z. Liu, J.S. Luo, C.M. Foster, Deposition and characterization of nanocrystalline diamond films, J. Vac. Sci. Technol. A 12 (1994) 1491.
[113] D.M. Gruen, S.Z. Liu, A.R. Krauss, J.S. Luo, X.Z. Pan, Fullerenes as precursors for diamond film growth without hydrogen or oxygen additions, Appl. Phys. Lett. 64 (1994) 1502.
[114] D.M. Gruen, S.Z. Liu, A.R. Krauss, X.Z. Pan, Buckyball microwave plasmas: fragmentation and diamond-film growth, J. Appl. Phys. 75 (1994) 1758.
[115] D.M. Gruen, Nanocrystalline diamond films, Annu. Rev. Mater. Res. 29 (1999) 211–259.
[116] D.M. Gruen, Ultrananocrystalline diamond in the laboratory and the cosmos, MRS Bull. 26 (2001) 771–776.
[117] W.D. Harkins, Energy relations of the surface of solids I. Surface energy of the diamond, J. Chem. Phys. 10 (1942) 268.
[118] S. Mandal, Nucleation of diamond films on heterogeneous substrates: a review, RCS Adv. 11 (2021) 10159.
[119] M. Lions, S. Saada, B. Bazin, M.A. Pinault, F. Jomard, F. Andrieu, O. Faynot, P. Bergonzo, Extreme insulating ultrathin diamond films for SOD applications: from coalescence modelling to synthesis, Diamond Relat. Mater. 19 (2010) 413.
[120] E.J.W. Smith, A.H. Piracha, D. Field, J.W. Pomeroy, G.R. Mackenzie, Z. Abdallah, et al., Mixed-size diamond seeding for low-thermal-barrier growth of CVD diamond on GaN and AlN, Carbon 167 (2000) 620.
[121] S. Handschuh-Wang, T. Wang, Y. Tang, Ultrathin diamond nanofilms-development, challenges, and applications, Small (2021) 2007529.
[122] M.A. Gebbie, H. Ishiwata, P.J. McQuade, V. Petrak, A. Taylor, C. Freiwald, J.E. Dahl, R.M.K. Carlson, A.A. Fokin, P.R. Schreiner, Z.-X. Shen, M. Nesladek, N.A. Melosh, Experimental measurement of the diamond nucleation landscape reveals classical and nonclassical features, Proc. Natl Acad. Sci. 115 (33) (2018) 8284–8289.
[123] H.-J. Lee, H. Jeon, W.-S. Lee, Ultrathin ultrananocrystalline diamond film synthesis by direct current plasma-assisted chemical vapour deposition, J. Appl. Phys. 110 (2011) 084305.
[124] T. Wang, S. Handschuh-Wang, P. Qin, Y. Yang, X. Zhou, Y. Tang, Enhancing the colloidal stability of detonation synthesized diamond particles in aqueous solutions by adsorbing organic mono-, bi- and tridentate molecules, J. Colloid Interface Sci. 499 (2017) 102.
[125] M. Couty, H.A. Girard, S. Saada, Nanoparticle adhesion and mobility in thin layers: nanodiamonds as a model, ACS Appl. Mater. Interfaces 7 (2015) 15752–15764.
[126] S. Stehlik, M. Varga, P. Stenclova, L. Ondic, M. Ledinski, J. Pangrac, O. Vanek, J. Lipov, A. Kromka, B. Rezek, Ultrathin nanocrystalline diamond films with silicon vacancy color centers via seeding by 2 nm detonation nanodiamonds, ACS Appl. Mater. Interfaces 9 (2017) 38842–38853.
[127] S. Mandal, E.L.H. Thomas, T.A. Jenny, O.A. Williams, Chemical nucleation of diamond films, ACS Appl. Mater. Interfaces 8 (2016) 26220.
[128] T. Yoshikawa, M. Reusch, K. Holc, D. Iankov, V. Zuerbig, A. Zukauskaite, C.E. Nebel, O. Ambacher, V. Lebedev, Enhanced actuation of nanocrystalline diamond microelectromechanical disk resonators with AlN layers, Appl. Phys. Lett. 108 (2016) 171903.
[129] Y.-C. Chen, C.-Y. Tsai, C.-Y. Lee, I.N. Lin, In vitro and in vivo evaluation of ultrananocrystalline diamond as an encapsulation layer for implantable microchips, Acta Biomater. 10 (2014) 2187.
[130] A. Qureshi, Y. Gurbuz, M. Howell, W.P. Kang, J.L. Davidson, Nanocrystalline diamond film for biosensor applications, Diamond Relat. Mater. 19 (2010) 457–461.
[131] S. Daboss, P. Knitell, C.E. Nebel, C. Kranz, Multifunctional boron-doped diamond colloid AFM probes, Small 15 (2019) 1902099.

[132] M. Ficek, M. Sobaszek, M. Gnyba, J. Ryl, L. Golunski, M. Smietana, J. Jasinski, P. Caban, R. Bodgdanowicz, Optical and electrical properties of boron doped diamond thin conductive films deposited on fused silica glass substrates, Appl. Surf. Sci. 387 (2016) 846–856.
[133] L. Huang, T. Wang, X. Li, X. Wang, W. Zhang, Y. Yang, Y. Tang, UV-to-IR highly transparent ultrathin diamond nanofilms with intriguing performances: anti–fogging, self-cleaning and self-lubricating, Appl. Surf. Sci. 527 (2020) 146733.
[134] M. Kosowska, D. Majchrowicz, J.K. Sankaran, M. Ficek, K. Haenen, M. Szczerska, Doped nanocrystalline diamond films as reflective layers for fiber-optic sensors of refractive index of liquids, Materials 12 (2019) 2124.
[135] M. Kosowska, D. Majchrowicz, M. Ficek, P. Wierzba, Y. Fleger, D. Fixler, M. Szczerska, Nanocrystalline diamond sheets as protective coatings for fiber-optic measurement head, Carbon 156 (2020) 104–109.
[136] H. Krysova, J. Barton, V. Petrak, R. Jurok, M. Kuchar, P. Cigler, L. Kavan, Efficiency and stability of spectral sensitization of boron-doped-diamond electrodes through covalent anchoring of a donor-acceptor organic chromophore (P1), Phys. Chem. Chem. Phys. 18 (2016) 16444–16450.
[137] A. Kovalenko, P. Ashcheulov, A. Guerrero, P. Heinrichova, L. Fekete, M. Vala, M. Weiter, I. Kratochvilova, G. Garcia-Belmonte, Diamond-based electrodes for organic photovoltaic devices, Sol. Energy Mater. Sol. Cells 134 (2015) 73–79.
[138] S.D. Janssens, S. Drijkoningen, K. Haenen, Ultra-thin nanocrystalline diamond membranes as pressure sensors for harsh environments, Appl. Phys. Lett. 104 (2014) 073107.
[139] J Achard, V Jacques, A Tallaire, Chemical vapour deposition diamond single crystals with nitrogen-vacancy centres: a review of material synthesis and technology for quantum sensing applications, J. Phys. D: Appl. Phys. 53 (2020) 313001.
[140] S. Stehlik, L. Ondic, M. Varga, J. Fait, A. Artemenko, T. Glatzel, A. Kromka, B. Rezek, Silicon-vacancy centers in ultra-thin nanocrystalline diamond films, Micromachines 9 (2018) 281.
[141] I. Aharonovich, S. Castelletto, D.A. Simpson, C.-H. Su, A.D. Greentree, S. Prawer, Diamond-based single-photon emitters, Rep. Prog. Phys. 74 (2011) 076501.
[142] K.D. Jahnke, A. Sipahigil, J.M. Binder, M.W. Doherty, M. Metsch, J.L. Rogers, N.B. Manson, M.D. Lukin, F. Jelezko, Electron-phonon processes of the silicon-vacancy centre in diamond, New J. Phys. 17 (2015) 043011.
[143] E. Neu, D. Steinmetz, J. Riedrich-Moller, S. Gsell, M. Fischer, M. Schreck, C. Becher, Single photon emission from silicon-vacancy colour centres in chemical vapour deposition nano-diamonds on iridium, New J. Phys. 13 (2011) 025012.
[144] Y. Mei, D. Fan, S. Lu, Y. Shen, X. Hu, SiV center photoluminescence induced by C=O termination in nanocrystalline diamond and graphite loops hybridized films, J. Appl. Phys. 120 (2016) 225107.
[145] J.O. Sofo, A.S. Chaudhari, G.D. Barber, Graphane: a two-dimensional hydrocarbon, Phys. Rev. B 75 (2007) 153401.
[146] S Ryu, MY Han, J Maultzsch, TF Heinz, P Kim, ML Steigerwald, et al., Reversible basal plane hydrogenation of graphene, Nano Lett. 8 (12) (2008) 4597–4602.
[147] D.C. Elias, R.R. Nair, T.M.G. Mohiuddin, S.V. Morozov, P. Blake, M.P. Halsall, et al., Control of graphene's properties by reversible hydrogenation: evidence for graphane, Science 323 (2009) 610.
[148] RR Nair, W Ren, R Jalil, I Riaz, VG Kravets, L Britnell, et al., Fluorographene: a two-dimensional counterpart of Teflon, Small 6 (24) (2010) 2877–2884.
[149] KS Subrahmanyam, P Kumar, U Maitra, A Govindaraj, KPSS Hembram, UV Waghmare, et al., Chemical storage of hydrogen in few-layer graphene, Proc. Natl. Acad. Sci. 108 (2011) 2674–2677.
[150] HL Poh, F Sanek, Z Sofer, M. Pumera, High-pressure hydrogenation of graphene: towards graphane, Nanoscale 4 (2012) 7006–7011.
[151] Z Yang, Y Sun, LB Alemany, TN Narayanan, WE. Billups, Birch reduction of graphite. Edge and interior functionalization by hydrogen, J. Am. Chem. Soc. 134 (2012) 18689–18694.
[152] RA Schäfer, JM Enlert, P Wehrfritz, W Bauer, F Hauke, T Seyller, et al., On the way to graphane-pronounced fluorescence of polyhydrogenated graphene, Angew. Chem. Int. Ed. 52 (2013) 754–757.
[153] Z Sofer, O Jankovsky, P Simek, L Soferova, D Sedmidubsky, M. Pumera, Highly hydrogenated graphene via active hydrogen reduction of graphene oxide in the aqueous phase at room temperature, Nanoscale 6 (2014) 2153–2160.
[154] L Zheng, Z Li, S Bourdo, F Watanabe, CC Ryerson, AS. Biris, Catalytic hydrogenation of graphene films, Chem. Commun. 47 (2011) 1213–1215.
[155] R Krishna, E Titus, LC Costa, JCJMDS Menezes, MRP Correia, S Pinto, et al., Facile synthesis of hydrogenated reduced graphene oxide via hydrogen spillover mechanism, J. Mater. Chem. 22 (2012) 10457–10459.
[156] JS Burgess, BR Matis, JT Robinson, FA Bulat, FK Perkins, BH Houston, et al., Tuning the electronic properties of graphene by hydrogenation in a plasma enhanced chemical vapour deposition reactor, Carbon 49 (2011) 4420–4426.
[157] Z Luo, T. Yu, K Kim, Z Ni, Y You, S Lim, et al., Thickness-dependent reversible hydrogenation of graphene layers, ACS Nano 7 (2009) 1781–1788.
[158] JD Jones, WD Hoffmann, AV Jesseph, CJ Morris, GF Verbeck, JM. Perez, On the mechanism for plasma hydrogenation of graphene, Appl. Phys. Lett. 97 (2010) 233104-1-233104-3.
[159] M Wojtaszek, N Tombros, A Caretta, PHM van Loosdrecht, BJ. van Wees, A road to hydrogenating graphene by a reactive ion etching plasma, J. Appl. Phys. 110 (2011) 063715-1-063715-6.
[160] G Diankov, M Neumann, D. Goldhaber-Gordon, Extreme Monolayer-selectivity of hydrogen-plasma reactions with graphene, ACS Nano 7 (2013) 1324–1332.
[161] A Felten, A Eckmann, JJ Pireaux, R Krupke, C. Casiraghi, Controlled modification of mono- and bilayer graphene in O_2, H_2 and CF_4 plasmas, Nanotechnology 24 (2013) 355705.
[162] L.A. Chernozatonskii, P.B. Sorokin, A. Kvashnin, D.G. Kvashnin, Diamane: simulation of the structure and properties, J. Exp. Theor. Phys. Lett. 90 (2009) 134–138.
[163] S. Rajasekaran, F. Abild-Pedersen, H. Ogasawara, A. Nilsson, S. Kaya, Interlayer carbon bond formation induced by hydrogen adsorption in few-layer supported graphene, Phys. Rev. Lett. 111 (2013) 085503-1-0585035.
[164] P.B. Sorokin, B.I. Yakobson, Two-dimensional diamond—diamane: current state and further prospects, Nano Lett. 21 (13) (2021) 5475–5484.
[165] D. Odkhuu, D. Sin, R.S. Ruoff, N. Park, Conversion of multilayer graphene into continuous ultrathin sp3-bonded carbon films on metal surfaces, Sci. Rep. 3 (2013) 3276-1-3276-7.
[166] L.A. Chernozatonskii, V.A. Demin, Diamond-like films from twisted few-layer graphene, JETP Lett. 115 (2022) 161–166.
[167] J. Zhou, Q. Wang, Q. Sun, X.S. Chen, Y. Kawazoe, P. Jena, Ferromagnetism in semihydrogenated graphene sheet, Nano Lett. 9 (11) (2009) 3867–3870.
[168] S.A. Redman, C. Chung, M.N.R. Ashfold, H atom production on a hot filament chemical vapour deposition reactor, Diamond Relat. Mater. 8 (1999) 1383–1387.
[169] Piazza F. Carbon nanotubes conformally coated with diamond nanocrystals or silicon carbide, methods of making the same and methods of their use. U.S. Patent 9,458,017, 2016.
[170] F. Piazza, G. Morell, J. Beltran-Huarac, G. Paredes, M. Ahmadi, M. Guinel, Carbon nanotubes coated with diamond nanocrystals and silicon carbide by hot–filament chemical vapor deposition below 200°C substrate temperature, Carbon 75 (2014) 113–123.
[171] L.A. Chernozatonskii, P.B. Sorokin, A.A. Kuzubov, B.P. Sorokin, A.G. Kvashnin, D.G. Kvashnin, et al., Influence of size effect on the electronic and elastic properties of diamond films with nanometer thickness, J. Phys. Chem. C 115 (2011) 132–136.
[172] L. Zhu, H. Hu, Q. Chen, S. Wang, J. Wang, F. Ding, Formation and electronic properties of hydrogenated few layer graphene, Nanotechnology 22 (2011) 185202.
[173] R.S. Ruoff, Personal perspectives on graphene: New graphene-related materials on the horizon, MRS Bull. 37 (2012) 1314–1318.
[174] Y. Hu, D. Li, Y. Yin, S. Li, G. Ding, H. Zhou, G. Zhang, The important role of strain on phonon hydrodynamics in diamond-like bi-layer graphene, Nanotechnology 31 (2020) 335711.
[175] S. Gupta, J.H. Yang, Yakobson B.I. Two-level quantum systems in two-dimensional materials for single photon emission, Nano Lett. 19 (1) (2019) 408–414.
[176] Z. Zheng, H. Zhan, Y. Nie, X. Xu, D. Qi, Y. Gu, Single layer diamond-A new ultrathin 2D carbon nanostructure for mechanical resonator, Carbon 161 (2020) 809–815.
[177] A.A. Balandin, Thermal properties of graphene and nanostructured carbon materials, Nat. Mater. 10 (2011) 569.
[178] J.E. Field, The mechanical and strength properties of diamond, Rep. Prog. Phys. 75 (2012) 126505.
[179] Z. Pan, H. Sun, Y. Zhang, C. Chen, Harder than diamond: superior indentation strength of wurzite BN and lonsdaleite, Phys. Rev. Lett. 102 (2009) 055503-1-055503-4.
[180] C. Feng, J. Xu, Z. Zhang, J. Wu, Morphology- and dehydrogenation-controlled mechanical properties in diamond nanothreads, Carbon 124 (2017) 9–22.
[181] J.C. Angus, F.A. Buck, M. Sunkara, T.F. Groth, C.C. Hayman, R. Gat, Diamond growth at low pressures, MRS Bull. 14 (10) (1989) 38–47.
[182] R. Haubner, B. Lux, Diamond grown by hot-filament chemical vapor deposition; state of the art, Diam. Relat. Mater. 2 (1993) 1277–1294.
[183] G.A. López, E.J. Mittemeijer, The solubility of C in solid Cu, Scr. Mater. 51 (2004) 1–5.
[184] N. Boutroy, Y. Pernel, J.M. Rius, F. Auger, H.J. von Bardeleben, J.L. Cantin, F. Abel, A. Zeinert, C. Casiraghi, A.C. Ferrari, J. Robertson, Hydrogenated amorphous carbon film coating of Pet bottles for gas diffusion barriers, Diam. Relat. Mater. 15 (4-8) (2006) 921–927.
[185] S. Hong, C-S Lee, M.-H. Lee, Y. Lee, K.Y. Ma, G. Kim, et al., Ultra-low dielectric-constant amorphous boron nitride, Nature 582 (2020) 511.